

Searching for the most powerful thermonuclear X-ray bursts with the *Neil Gehrels Swift* Observatory

J. J. M. in 't Zand¹, M. J. W. Kries^{1,2}, D. M. Palmer³, and N. Degenaar⁴

¹ SRON Netherlands Institute for Space Research, Sorbonnelaan 2, 3584 CA Utrecht, The Netherlands
e-mail: jeanz@sron.nl

² Dep. of Physics, Utrecht University, PO Box 80000, 3508 TA Utrecht, The Netherlands

³ Los Alamos National Laboratory, B244, Los Alamos, NM 87545, USA

⁴ Anton Pannekoek Instituut for Astronomy, University of Amsterdam, Science Park 904, 1098 XH Amsterdam, The Netherlands

Received 18 September 2018 / Accepted 25 October 2018

ABSTRACT

We searched for thermonuclear X-ray bursts from Galactic neutron stars in all event mode data of the *Neil Gehrels Swift* Observatory collected until March 31, 2018. In particular, we are interested in the intermediate-duration bursts (shell flashes fueled by thick helium piles) with the ill-understood phenomenon of strong flux fluctuations. Nine such bursts have been discussed in the literature to date. *Swift* is particularly suitable for finding additional examples. We find and list a total of 134 X-ray bursts; 44 are detected with BAT only, 41 with XRT only, and 49 with both. Twenty-eight bursts involve automatic slews. We find 12 intermediate-duration bursts, all detected in observations involving automatic slews. Five show remarkably long Eddington-limited phases in excess of 200 s. Five show fluctuations during the decay phase; four of which are first discussed in the present study. We discuss the general properties of the fluctuations, considering also 7 additional literature cases. In general two types of fluctuations are observed: fast ones, with a typical timescale of 1 s and up and downward fluctuations of up to 70%, and slow ones, with a typical timescale of 1 min and only downward fluctuations of up to 90%. The latter look like partial eclipses because the burst decay remains visible in the residual emission. We revisit the interpretation of this phenomenon in the context of the new data set and find that it has not changed fundamentally despite the expanded data set. It is thought to be due to a disturbance of the accretion disk by outflowing matter and photons, causing obscuration and reflection due to Thomson scattering in an orbiting highly ionized cloud or structure above or below the disk. We discuss in detail the most pronounced burster SAX J1712.6–3739. One of the bursts from this source is unusual in that it lasts longer than 5600 s, but does not appear to be a superburst.

Key words. X-rays: binaries – X-rays: bursts – accretion, accretion disks – X-rays: individuals: SAX J1712.6–3739 – X-rays: individuals: 4U 1850–087 – X-rays: individuals: Swift J1734.5–3027

1. Introduction

One of the brightest phenomena in the keV X-ray sky is the Type I X-ray burst phenomenon (e.g., [Grindlay et al. 1976](#); [Swank et al. 1977](#)) with peak fluxes sometimes reaching $10^{-6} \text{ erg s}^{-1} \text{ cm}^{-2}$ (1–20 keV). We refer to these simply as X-ray bursts or bursters. They are due to thermonuclear shell flashes on neutron stars with a relatively low magnetic field, during which the hydrogen and helium accreted from a Roche-lobe overflowing companion star in a compact low-mass X-ray binary is burned (e.g., [Hansen & van Horn 1975](#); [Maraschi & Cavaliere 1977](#); [Joss 1977](#)). The thermonuclear runaway commences within seconds, after which the neutron star cools on a timescale of 10 s–10 h, depending on the ignition depth. During the flashes, the photosphere reaches a temperature on the order of 10 MK and radiates predominantly in X-rays (for reviews, see, e.g., [Lewin et al. 1993](#); [Strohmayer & Bildsten 2006](#); [Galloway & Keek 2017](#)). The nuclear power generated in such a flash can be excessive, reaching a level where the radiation pressure gradient overcomes the strong gravitational pull by the neutron star. In other words, the Eddington limit is reached. A wind and shell may be blown from the neutron star. The outflowing photon and matter flux interacts with the accretion flow/disk and can seriously disturb it, depending on its geometry ([in 't Zand et al. 2011](#)).

As of March 31, 2018, 111 bursting neutron stars were known in the Galaxy (see [Table A.1](#))¹. The number of bursts detected per neutron star varies widely. Since the burst process is fueled by accretion, the momentary accretion rate determines to a large extent the recurrence time. Transiently accreting neutron stars can only burst when there is accretion, which on average occurs a few percent of the time (cf., [Yan & Yu 2015](#)) or maybe somewhat more ([Degenaar & Wijnands 2010](#)). Neutron stars that accrete persistently on a timescale of a human life can burst at a rate anywhere between roughly once per hour to once per month.

Three major kinds of X-ray bursts can be identified:

1. common X-ray bursts (e.g., [Lewin et al. 1993](#)), with recurrence times of a few hours and durations of tens of seconds. The accretion rate is larger than a few percent of the Eddington limit. The bursts may be fueled by a mixture of hydrogen and helium or only helium. In the latter case, the luminosity often reaches the Eddington limit and the photosphere is seen to expand;
2. intermediate-duration bursts (e.g., [in 't Zand et al. 2005, 2007](#); [Cumming et al. 2006](#); [Falanga et al. 2008](#)), with recurrence times of many weeks and durations of tens of minutes. The accretion rate is smaller than 1% of the Eddington

¹ See also <https://www.sron.nl/~jeanz/bursterlist.html>

limit, except in GX 17+2 (Kuulkers et al. 2002a). They are thought to be fueled by a large pile of helium. The combination of helium as a fuel, which burns relatively quickly, and the amount of fuel provides a circumstance where the nuclear power is many times higher than the Eddington limit;

3. superbursts with recurrence times of about one year and durations of about one day. These bursts are seen to occur at a wide range of accretion rates (for a recent review, see in 't Zand 2017). They are thought to be fueled by carbon at a column depth that is about 10^3 larger than for common He/H bursts (Cumming & Bildsten 2001; Strohmayer & Brown 2002). Superbursts are usually sub-Eddington, due to the smaller energy output per nucleon, the smaller mass fraction of the carbon in the ignited layer, and the longer heat diffusion time.

Some long bursts have very strong flux fluctuations with respect to the typical power-law decay of the burst (in 't Zand et al. 2014a, 2017), with amplitudes above and below the cooling curve of order 50% on timescales of 1 s–1 min. So far, nine such bursts have been reported (van Paradijs et al. 1990; Strohmayer & Brown 2002; in 't Zand et al. 2005, 2008, 2011; Palmer 2011; Molkov et al. 2005; Degenaar et al. 2013; Barrière et al. 2015) as measured with the instruments Ginga-LAC, INTEGRAL-JEM-X, *BeppoSAX*-WFC, RXTE-PCA, *Swift*-XRT, and NuSTAR (for a recent overview, see Degenaar et al. 2018). The common characteristics are that the fluctuations are at least 10% and that they occur with some delay (order one minute) after the Eddington-limited phase. The nature of this phenomenon is not fully understood, but it seems clear that the accretion disk plays a role. In order to get a more complete understanding of the phenomenon, more data would be useful. *Swift* is an efficient tracker of these bursts. Therefore, we set out to investigate all *Swift* XRT and BAT data on X-ray bursts.

To detect rare kinds of bursts it is crucial to use wide-field imaging devices. There are two kinds of wide-field devices. There are those with a limited field of view (FOV) that scan the sky. Examples are RXTE/ASM and ISS/MAXI that scan >80% of the sky every 1.5 h. This revisit time is sufficiently short to identify superbursts (Kuulkers et al. 2002b; Serino et al. 2017; Iwakiri et al. 2018), but not intermediate-duration bursts. Second, there are devices with truly wide FOVs, such as the *BeppoSAX* Wide Field Camera instrument (WFC; Jager et al. 1997), that are efficient in detecting bursts of all durations.

The spectra of X-ray bursts have a peak temperature of $kT = 2.0$ – 2.5 keV, which implies that the photon spectrum peaks at 3–4 keV and the energy spectra at 6–7.5 keV. Thus, the detector of a wide-field device should preferably be able to detect photons in the 2–10 keV range, such as *BeppoSAX*/WFC (FOV 8% of the sky) or INTEGRAL/JEM-X (0.3%).

There are other wide-field devices in orbit, but they are active at somewhat unfavorable bandpasses. They include the non-imaging *Fermi* Gamma-ray Burst Monitor (GBM; 8 keV–1 MeV), which has 100% sky coverage (being limited only by the Earth obscuring a third of the sky), and the imaging Burst Alert telescope on the *Neil Gehrels Swift* Observatory (BAT; 15–~150 keV) with a FOV of 18% of the sky and mostly pointed away from Earth. The sensitivities of these devices on a 5 s timescale to a 2.5 keV blackbody are about 1 Crab (Jenke et al. 2016) and 100 mCrab, respectively. The better sensitivity of the BAT is due to a larger detector and the imaging capability. The GBM detects about 250 bursts per year during the phases when the bursts are hotter than $kT = 2.5$ keV (Jenke et al. 2016). This

implies that superbursts can hardly be detected because the temperature peaks at lower values.

While the detection capabilities of GBM and BAT are good, the diagnostic capabilities are limited. Both instruments are only able to detect the hottest phases of X-ray bursts, losing the signal quickly during the burst decay where most of the fluence is emitted. The BAT has one important advantage: it can trigger automatic pointings of the *Swift* X-Ray Telescope (XRT) at the burst. The XRT is very sensitive because it is a focusing telescope. Automatic slews typically happen within about 100 s. This implies that the BAT+XRT combination is particularly efficient in detecting intermediate-duration bursts. These bursts are super-Eddington and therefore reach the highest possible temperatures. Also, they last a long time so that they are easily picked up with XRT despite the response delay.

We estimate that 12–14 thousand X-ray bursts have been detected since the advent of X-ray astronomy in the 1960s. Judged from a subset of one thousand well-observed cases (Galloway et al. 2008), it appears that some 20% show evidence of the radiation-pressure effect mentioned above. This evidence pertains to a temporary increased emission region size as derived from the spectrum. This is called photospheric radius expansion (PRE). In addition, there are a few (~1%) PRE X-ray bursts that show superexpansion, where the expansion is so large (with a radius growing from ~10 km to $\geq 10^3$ km) that the temperature drops out of the 1–10 keV bandpass and the illusion of a precursor event is created (in 't Zand & Weinberg 2010). Many intermediate-duration bursts seem to have superexpansion if the sensitivity is sufficient to detect it given the short nature.

We set out to obtain an overview of burst detections with *Swift*-BAT and XRT for which event data is available so that light curves can be followed to small fluxes and intermediate-duration bursts can be distinguished, and to concentrate on those that show fluctuations. In Sect. 2 we present the relevant details of the *Swift* instrumentation and operations, in Sect. 3 the approach used to search for bursts, in Sect. 4 our analysis of all relevant new data, in Sect. 5 an overview of relevant data from the literature, in Sect. 6 a comparative analysis of all intermediate-duration bursts and fluctuations, and in Sect. 7 a discussion of the results and the implications for the model of the fluctuations.

2. Instrumentation and follow-up algorithm

The *Neil Gehrels Swift* Observatory is a NASA Medium Explorer mission launched on November 20, 2004. The main goal of the observatory is to search and study gamma-ray bursts (GRBs; Gehrels et al. 2004), but it is also very successful in the study of X-ray bursts (e.g., the discovery of 13 new X-ray burst sources, see Appendix A). To observe GRBs and their afterglows, *Swift* has three instruments: the wide-field BAT (Barthelmy et al. 2005), and the narrow-field X-ray (XRT; Burrows et al. 2005) and Ultraviolet/Optical Telescopes (UVOT; Roming et al. 2005).

The BAT (Barthelmy et al. 2005) is a coded aperture camera with a large FOV of 2.3 sr (for a response larger than 5% of the maximum), which is 18% of the entire sky, an angular resolution of 17 arcmin (on-axis), and a localization accuracy of 1–4 arcmin (depending on the strength of the signal above the background). The CdZnTe detector array provides a 15–150 keV bandpass with a resolution of about 7 keV. The BAT is used to detect GRBs, automatically localizing them on board and triggering the observatory to automatically slew the optical axis of the satellite with the co-aligned narrow-field instruments to the GRB.

The XRT (Burrows et al. 2005) is an X-ray telescope active between 0.2 and 10 keV with an angular resolution of 18–22'' (HPD; 1.5–8 keV), a typical location accuracy of 3'', a 600×600 pixels CCD camera with a spectral resolution of 140 eV at 5.9 keV and an effective area of 125 cm² at 1.5 keV and 20 cm² at 8 keV. The sensitivity is about 3×10^{-11} erg cm⁻² s⁻¹ in 10 s. The CCD full-image readout time is 2.5 s, but the CCD can also be read out in the Windowed Timing mode, when the columns are collapsed and limited to a width of 8'. The readout time then reduces to 1.7 ms, allowing the measurement of photon intensities of a few hundred counts per second with a pile-up fraction of less than 1%.

The onboard software uses two algorithms to identify a trigger. First, it checks for temporary excesses in the photon rates above the background and persistent cosmic sources in (sections of) the detector array in four channel ranges (15–25, 15–50, 25–100, 50–150 keV) and on timescales between 4 ms and 32 s. When a photon rate increase is detected above a certain significance (from 5 to 12 σ depending on energy and timescale) the excess counts in each detector pixel are deconvolved to give a sky image using an FFT-based algorithm that takes 6 s. Each significant peak in the sky image is then reanalyzed with a photon back-projection algorithm that provides a higher accuracy determination of the source location, flux, and significance. In addition, the software analyzes images on 64 s, 320 s, and full pointing timescales to search for sources that do not cause rapid rate variations on the shorter timescales.

Each peak location is compared to an onboard catalog of 1300 known sources (including most known bursters). If the location of a significant image peak is not found in the catalog, it is declared to be a GRB. If the location is found in the catalog, a threshold and a merit parameter are extracted from that source's catalog entry. The image flux (or in some cases the fluence) is compared to the threshold to determine whether the detection is interesting. An interesting detection results in immediate ground notification, extended event-data recording, and possible pointing follow-up. Most source detections are not interesting in this sense; the Crab and other bright sources are detected whenever they are in the FOV, and so their thresholds are set so that typical emission is not considered interesting. Likewise, large numbers of bursts from known sources are detected and recorded, but usually do not trigger a further response. After a detection, the catalog threshold for that source is automatically set to double the measured value so that further activity at the same level is not considered interesting until the threshold is manually commanded back to a lower level. This prevents excess resource use when a transient source appears and persists above its original interesting threshold.

If a source detection is considered interesting, that source's merit parameter is combined with other parameters (such as its location relative to the Sun and Moon exclusion zones) to give an overall Figure of Merit (FoM) value, and the source becomes *Swift*'s new Automated Target (AT) unless there is already an active AT with a higher FoM. *Swift* continuously tests whether the current AT is in the observable part of the sky and, if so, compares its FoM to that of the Pre-Planned Science Target (PPST) scheduled for that time. If the AT has a higher FoM, *Swift* slews to the AT and continues pointed observations until it is no longer observable, a higher-FoM PPST takes precedence, or the AT completes a pre-determined total observation time. These pointed observations allow XRT and UVOT follow-up observation within 100 s after detection (*Swift*'s typical slew time) if the source's merit is sufficient.

In the first five years of the mission, the FoM for known sources (including X-ray bursters, unless not yet known as such) were set to very low values and they would not be observed with the XRT, unless accidentally because the onboard catalog was not up to date. In 2009 this approach changed. A few other targets received higher priority. Bursters with very low burst rates were allowed to be followed up (prior to May 2009 M15 X-2, 1RXS J170854.4–321857, 1RXS J171824.2–402934, 4U 1722–30, SLX 1737–282 and SAX J1752.3–3138; Markwardt, priv. comm.) next to of course new bursters.

3. Search

We are looking for rare kinds of X-ray bursts that have coverage in the sub-10 keV band. Such coverage is necessary because fluctuations have only been seen in the tails of bursts when the temperature may be too low for useful data in the >15 keV band. We are most likely to find these bursts among BAT triggers that resulted in automatic slews and have positions coincident with known X-ray bursters.

We first searched for detections of X-ray bursts with BAT that triggered the instrument into downloading event data, by querying the *Swift* Master Catalog at HEASARC for all observations with BAT event data for more than 5 s. This image-encoded data, sampled at 0.1 ms, enables the verification of a true burst signal from the location of a bonafide X-ray burster. BAT provides event mode data whenever it is triggered by one of the onboard rate or image trigger algorithms. Depending on the follow-up script as specified per source, either 21 min of such event mode data are downloaded or 40 s. Bursts that result in an AT will always have 21 min of event mode data available.

Our query on March 31, 2018, yielded 2319 observations, including 985 gamma-ray bursts. We downloaded the mask-tagged light curves for the triggers and compared the RA and Dec coordinates of the trigger object with those of all known X-ray bursters (see Table A.1). With a match within 0.2 deg, this brought the list down to 96 events. We investigated the light curves to search for a clear burst signal and found 70.

28 of these bursts with BAT event data were slewed to and 25 have XRT data showing the later phases of the burst. Those lacking an XRT detection are 2005-02-24, 2008-03-18 and 2017-07-28. In two cases, XRT was already observing the source and the burst is completely covered with XRT. The 28 bursts are listed in Table 1 and the BAT and XRT light curves are presented in Fig. 1. Five of these 28 bursts have not been reported elsewhere (2005-02-24, 2008-03-18, 2008-03-31, 2011-06-19 and 2012-08-13). 12 bursts have been discussed in some detail in papers. 11 have merely been reported in GCN circulars or Astronomical Telegrams. The 28 bursts are from 24 sources. Three bursts are from a single source: SAX J1712.6–3739.

Additionally, we searched all XRT data of the 111 currently known Galactic X-ray bursters for X-ray bursts and found 65 additional bursts for a total of 90 bursts detected with XRT (see Table A.1). Therefore, we count 134 detections of X-ray bursts with event data from BAT or XRT; 49 of these have both BAT and XRT detections (25 as a result of a slew) while 41 have only XRT detections and 44 have only BAT detections. A total 69 out of the 134 have triggered BAT, yielding event mode data, while the remaining 65 bursts were first found in XRT data for which 21 times a signal was detected in non-event-mode data from BAT.

It should be noted that *Swift* detects many more X-ray bursts with BAT, but most are below the threshold for triggering BAT

Table 1. Overview of the 28 BAT-triggered bursts from 24 sources with coverage by the XRT, ordered by observation date.

Object	Trigger number	Trigger time (UTC)	Peak flux ($10^{-1} \text{ c s}^{-1} \text{ cm}^{-2}$)	Start XRT data after burst onset (s)	Duration $t_{5\%}$ (s)	Duration touch down (s)	Pre-cursor? (s)	Intermediate?	Reference
4U 1812-12	106799	2005-02-24 12:40:45	0.64(7)	160	<160	21	15	Y	
Swift J1749.4-2807	213190	2006-06-02 23:54:34	3.1(2)	90	<90	20	7		Wijnands et al. (2009)
1A 1246-588	223918	2006-08-11 02:59:56	2.0(2)	230	290	70	40	Y	in 't Zand et al. (2008)
SAX J1810.8-2609	287042	2007-08-05 11:27:26	2.1(2)	80	100	23	14	Y	Degenaar & Wijnands (2013)
XTE J1810-189	306737	2008-03-18 22:32:52	0.65(14)	100	<100	10	0		
IGR J17473-2721	308196	2008-03-31 09:03:33	1.7(2)	<0	75	25	10	Y	
1RXH J173523.7-35401	311603	2008-05-14 10:32:37	1.0(1)	250	>250	240	200	Y	Degenaar et al. (2010)
XTE J1701-407	317205	2008-07-17 13:29:59	3.1(2)	140	190	125	55	Y	Linares et al. (2009)
XTE J1701-407	318166	2008-07-27 22:31:20	2.0(2)	120	<110	15	10		Linares et al. (2009)
IGR J17511-3057	371210	2009-09-30 18:31:57	1.6(2)	50	<50	20	10		Bozzo et al. (2009)
SAX J1712.6-3739	426405	2010-07-01 14:55:41	1.7(2)	100	140	30	20		Strohmayer & Baumgartner (2010)
XTE J1810-189	455640	2011-06-19 00:59:37	0.75(12)	300	750	400	200	Y	
Swift J185003.2-0056	456014	2011-06-25 00:06:08	2.4(3)	100	<100	40	10		Degenaar et al. (2012a)
SAX J1712.6-3739	504101	2011-09-26 20:11:29	1.6(2)	180	1050	315	190	Y	Palmer (2011)
Swift J1922.7-1716	506913	2011-11-03 14:12:13	2.2(3)	120	<120	50	20	Y	Degenaar et al. (2012a)
IGR J17062-6143	525148	2012-06-25 22:42:32	1.6(3)	260	1300	420	220	Y	Degenaar et al. (2013)
XMM J174457-2850.3	530588	2012-08-11 04:43:54	2.1(2)	95	130	75	55	Y	Degenaar et al. (2014)
Swift J174805.3-244637	530808	2012-08-13 09:13:34	1.5(2)	90	<90	35	15	Y	
IGR J18245-2452	552369	2013-03-30 15:10:38	0.57(17)	120	Rise!	130	125	Y	Barthelmy et al. (2013)
Swift J1734.5-3027	569022	2013-09-01 09:13:17	1.8(2)	145	600	155	75	Y	Bozzo et al. (2015)
MAXI J1421-613	584155	2014-01-18 08:39:20	0.89(16)	<0	30	15	5	Y	Serino et al. (2015)
4U 1850-087	591237	2014-03-10 21:05:00	2.0(2)	610	1400	840	530	Y	in 't Zand et al. (2014a)
SAX J1712.6-3739	609878	2014-08-18 17:10:04	1.1(1)	270	>5530	>800	540	Y	Cummings et al. (2014)
4U 0614+09	631747	2015-02-19 16:42:24	8.2(4)	85	<120	6	3		Breeveld et al. (2015)
SAX J1808.4-3658	637765	2015-04-11 19:36:25	6.3(5)	40	50	25	7		Malesani et al. (2015)
IGR J00291+5934	650221	2015-07-25 02:12:05	3.2(6)	110	270	20	10	Y	De Falco et al. (2017)
SAX J1806.5-2215	745022	2017-04-01 19:00:53	0.81(14)	205	550	250	130	Y	Barthelmy et al. (2017a)
Swift J181723.1-164300	765081	2017-07-28 16:57:58	2.9(5)	80	<80	15	7	Y	Barthelmy et al. (2017b)

Notes. The bold typeset entries are bursts with fluctuations. All times are with a typical uncertainty of 1–5 s.

into a mode that provides imaged light curves for more than a few seconds to the ground at sufficient time resolution of ≤ 1 s or for triggering an automatic slew by *Swift*. These bursts do not allow to distinguish intermediate-duration bursts. They will be discussed in a forthcoming paper.

BAT light curves of thermonuclear X-ray bursts have a faster decay than in the classical 1–10 keV bandpass. Due to the 15 keV low-energy threshold and the 3 to <1 keV cooling of the burst, BAT loses the signal fast. BAT light curves can be divided in three classes: (1) fast rise, slow decay, (2) slow rise, fast decay and (3) precursor followed by slow rise and fast decay. Classes 2 and 3 are PRE bursts. Class (2) is more common among PRE bursts than in the classical band, again because of the BAT bandpass. Sometimes PRE bursts show a rise lasting up to minutes. PRE is characterized by a relatively short phase of expansion (a few seconds) followed by a slow phase of contraction until the photosphere shows a minimum in the emission region size as measured through the blackbody radius and a maximum in the spectral hardness as measured through the blackbody temperature (e.g., Lewin et al. 1993). This is known as the touchdown point. Due to the BAT spectral response, the PRE phase is observed as a slow rise in the BAT-measured flux. The touchdown point is followed by a decay because of a decreasing bolometric flux and spectral hardness.

The BAT trigger times are the start times of time intervals over which the trigger criterion is assessed, ranging from 4 ms to the duration of a full pointing. They are not necessarily equal to the start time of the bursts. To estimate the burst start time we qualitatively determine where the slope of the BAT light curve rise intersects the pre-burst flat level. Start times are

not determined very accurately and are estimated to have a 5 s uncertainty.

Of interest here are intermediate-duration bursts. The definition of these bursts naturally depends on the duration. On the one hand, it is a somewhat difficult parameter to measure; often there is only partial coverage in X-rays with XRT. On the other hand, there is no generally accepted threshold for duration above which we speak of intermediate-duration bursts. We define a duration as the length of time $t_{5\%}$ that the flux stays above 5% of the peak flux (see also in 't Zand et al. 2017). To be able to determine this with BAT and partial XRT data, we assume that the 15–25 keV BAT-measured peak flux happens at touchdown when the blackbody temperature peaks at about 3 keV (e.g., Galloway et al. 2008). For such a spectrum, a flux of $0.1 \text{ c s}^{-1} \text{ cm}^{-2}$ in BAT (15–25 keV) is equivalent to roughly 400 c s^{-1} in XRT (full bandpass and $N_{\text{H}} < 6 \times 10^{21} \text{ cm}^{-2}$). From the actual BAT peak flux we calculate what the 5% level is for the XRT, determine or estimate through extrapolation, if sensible, at what time the flux decays through that level, determine when the burst starts to rise above that level, and measure how much time passes between the two points in time. For a time profile consisting of a fast rise and an exponential decay, $t_{5\%}$ is 3 times the exponential decay time (the factor of 3 is equal to $-\ln(0.05)$). We define intermediate-duration bursts as $t_{5\%} > 150$ s, or an exponential decay time that is longer than 50 s. This is commensurate with durations longer than expected for common X-ray bursts (e.g., Fig. 1 in in 't Zand et al. 2017). We find 12 such cases in our BAT+XRT sample of 28 (see Table 1). This shows that BAT, thanks to the high temperatures of intermediate-duration bursts, is quite efficient in detecting them. In the 44 BAT-only bursts, there is one additional case of an intermediate-duration

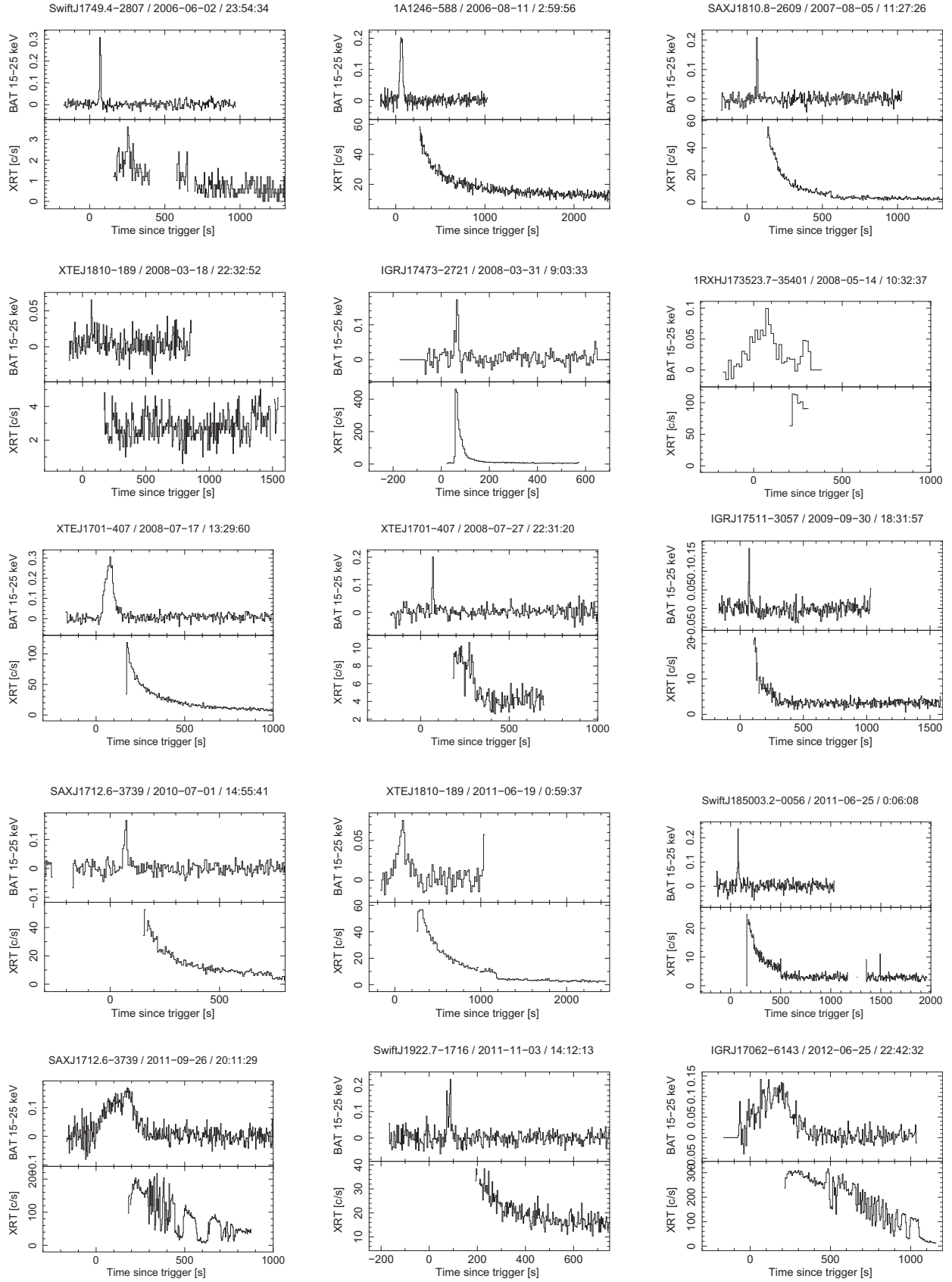


Fig. 1. BAT and XRT light curves of all 28 X-ray bursts with BAT event files and followed up with XRT, except 4U 1812-12/2005-02-24 because its XRT coverage is sparse. The BAT light curves are normalized and corrected for a changing pointing due to the slews. The XRT data are for the complete detector and without corrections for pile-up or background. The steps that can sometimes be seen in XRT data are due to a switch in CCD data collection mode with different pile-up fractions.

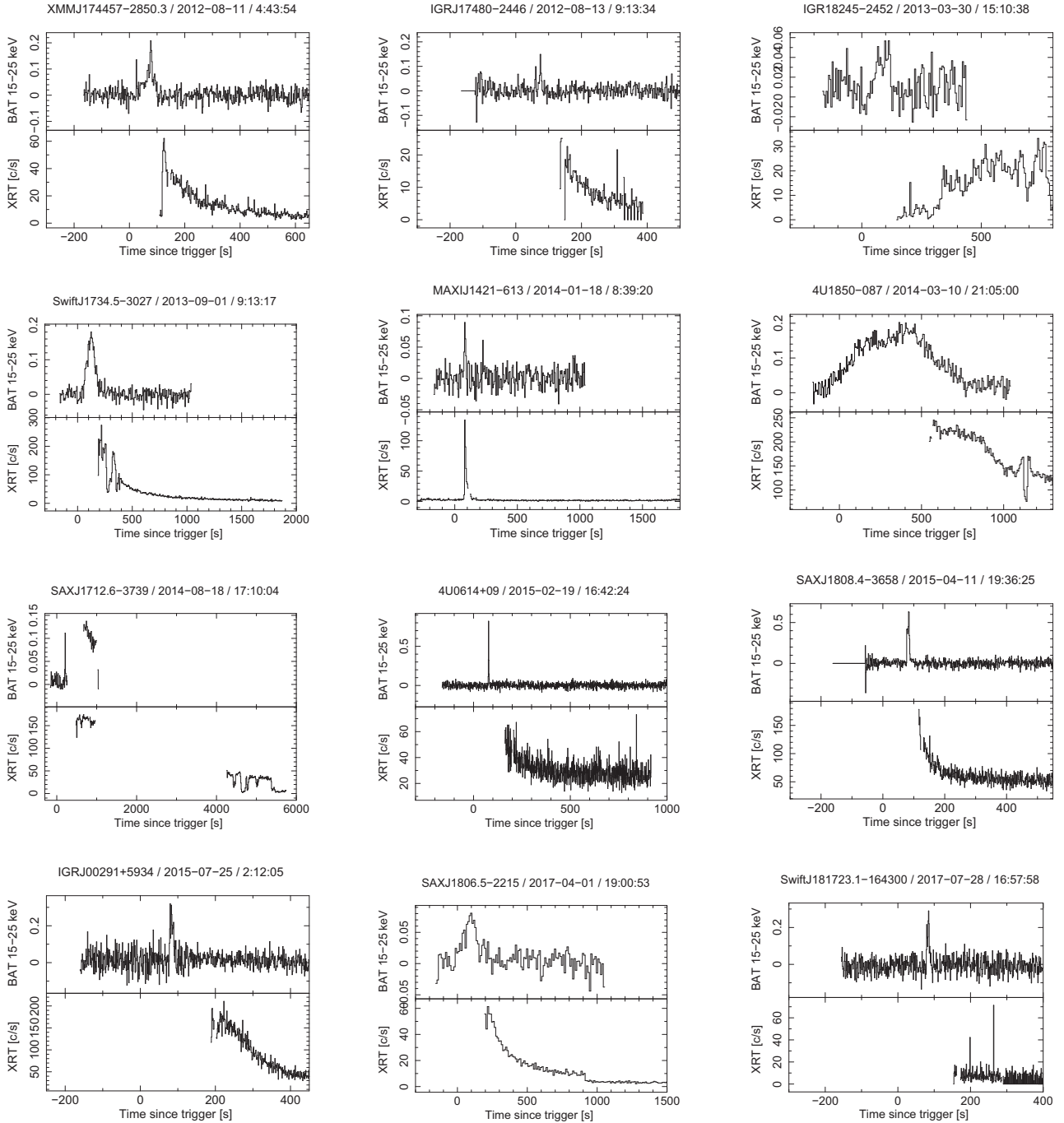


Fig. 1. continued.

burst because the rise time is very long: 80 s. This is a burst from XTEJ1701–407 on 2018-03-09. In the 90 XRT bursts, there are two more bursts with an e-folding time in excess of 50 s: one burst from GS 1826–24 on October 21, 2009, and one burst from 1RXS J180408.9–342058 on March 31, 2015. However, we regard these as examples of prolonged H-burning due to rapid proton captures (e.g., in *t* Zand et al. 2017) instead of cooling after a deep ignition as per intermediate-duration burst.

There are some exceptional cases among the intermediate-duration bursts. Five are longer than $t_{5\%} = 750$ s: two (out of three) bursts from SAX J1712.6–3739 (1050 and >5530 s), one from 4U 1850–087 (1400 s), XTEJ1810–189 (750 s) and IGR J17062–6143 (1300 s). These values approach those of bursts from SLX 1735–269 (~1600 s, Molkov et al. 2005) and

SLX 1737–282 (~1800 s, in *t* Zand et al. 2002). The longest burst from SAX J1712.6–3739 is extremely long (>5530 s). It looks somewhat like a superburst, but we argue that it is not (see Sect. 7.2). If we interpret the peak of the BAT light curve as the touchdown point at the end of the PRE phase, very long PRE phases are noticeable in some X-ray bursts: 530 s for 4U 1850–087, 220 s for IGR J17062–6143, and 200 s for XTEJ1810–189 and 1RXH J173523.7–35401. For the literature burst from SLX 1735–269 the time is 450 s (Molkov et al. 2005).

There are six bursts, marked in bold in Table 1, that show strong flux fluctuations in the XRT data during the decay, reminiscent of such features seen earlier in WFC and PCA data (in *t* Zand et al. 2005, 2008, 2011). In the following we focus on these bursts, all of which are intermediate-duration bursts.

4. Data analysis and results

We present an analysis of the XRT data of the six bursts with fluctuations (marked in bold in Table 1). The analysis pertains to the light curve and spectrum. We start by making some general notes about how we extracted the data and what the results of a standard analysis show, and continue with a discussion of the six bursts individually in order of right ascension. It is noted that to date only the fluctuations in the XRT data from IGR J17062–6143 have been completely analyzed and published (Degenaar et al. 2013). This is also the burst with the highest quality XRT data.

4.1. General notes

While the BAT light curves are continuous, the XRT light curves of the six cases under investigation lack the burst onset as they are automatic slew targets. Due to the high intensity, all interesting data were acquired in Windowed Timing mode and we only investigate these data. In this mode, the detector is less susceptible to pile-up at high count rates. The downside is that imaging information is lost in one direction and the background is accordingly higher.

XRT source data were extracted from a circular region of radius 90 arcsec around the source, the background data from all detector areas at least 120 arcsec from the source. The background data were normalized to the source extraction region area.

For spectral data, we only used grade-0 photons and excluded a central region of 3.5 arcsec radius around the source position that may be affected by pile-up. We believe that pile-up effects are minor for the observed photon detection rates at the employed XRT Window Mode with a readout time of only 1.7 ms per CCD column, but even minor pile-up effects may be noticeable in spectral data. We expect pile-up fractions of no more than 1% given the maximum count rates of about 300 cs^{-1} (as derived from HEASARC's WebPIMMS tool, see also Romano et al. 2006). When extracting light curves, we did not exclude the central region because we wanted to use as many photons as possible. Analysis of spectra was performed with XSPEC version 12.9.1 (Arnaud 1996). Spectral data below 0.7 keV were ignored as suggested by the XRT calibration digest². Spectra were background subtracted; light curves were not. We binned spectra with the `grppha` tool. The minimum number of counts per energy channel was set to 15 to allow use of chi-squared as a goodness of fit. Spectra were sometimes further binned in XSPEC for plot aesthetics.

We calculated two hardness ratios from the XRT data: the ratio of the flux in 2.5–10 keV to that in 0.3–2.5 keV and the ratio of the flux in 4.0–10 keV to that in 2.0–4.0 keV. For this, we generally use a bin time of 5 s. If the data are relatively noisy, we experimented with a longer bin time to find a binning that decreases the noise level but sustains some resolution to allow seeing evolution, if present.

Time-resolved spectroscopy is done by extracting spectra in a series of time intervals that are matched to the fluctuations in the light curves. The spectra are modeled with an absorbed Planck function (`wabs*bodyrad` in XSPEC jargon) in which N_{H} is fixed to the literature value (see Table 2). This sometimes implies small time intervals in which derived spectral parameters may be ill constrained. The unabsorbed bolometric flux is calculated using the `cflux` model in XSPEC between 0.1 and 30 keV.

4.2. General analysis of all bursts

For all six bursts, time profiles of full-bandpass XRT intensity and both hardness ratios are drawn in Fig. 2. It should be noted that 1) the light curves of the first burst from SAX J1712.6–3739 and the burst from IGR J17062–6143 show fast fluctuations up and down, while those of the others show only slow dips or partial eclipse-like features (except IGR J18245–2452); 2) the fluctuations in the light curves are traceable in the 2.5–10 keV/0.3–2.5 keV hardness ratio, but not in 4–10 keV/2–4 keV. In other words, the fluctuations in the bursts are approximately achromatic above 2.5 keV and not below (cf. in 't Zand et al. 2011; Degenaar et al. 2013). We note that only IGR J17062–6143, Swift J1734.5–3027, IGR J18245–2452, and 4U 1850–87 have low enough interstellar absorption to have ample signal below 2 keV; 3) the light curve of IGR J18245–2452 shows no decaying trend. Its association with burst emission is uncertain (see Sect. 4.6).

We carried out a standard spectral data reduction procedure on all six bursts. Time intervals were determined from 1 s resolution intensity time histories when the flux is below the anticipated decay trend and when it is high. The latter condition applies for times when there are fast upward fluctuations (in SAX J1712.6–3739 and IGR J17062–6143) and for times when there are no slow dips. Both “lo” and “hi” spectra are fitted with a single absorbed blackbody, neglecting non-burst emission from the same source. This non-burst emission is not measurable because there is no pre-burst or immediate post-burst data, but its flux is often 10^2 times smaller, as we argue below. The results are shown in Fig. 3 and Table 2. We note that 1) IGR J17062–6143 exhibits a strong sub-2 keV component (see also Degenaar et al. 2017; van den Eijnden et al. 2018). This detection in our sample may be a selection effect because it has the most photons and the lowest N_{H} ; 2) the blackbody temperatures of the lo and hi spectra often differ slightly (on a level of up to 5σ) and there is no consistent behavior that the lowest or highest temperatures coincide with the lo spectra; 3) spectral shapes for lo and hi periods are similar above 2 keV; and 4) the data for the burst from IGR J18245–2452 looks out of the ordinary, i.e., it is substantially cooler.

4.3. Burst from IGR J17062-6143

IGR J17062–6143 is an accretion-powered millisecond pulsar with a spin frequency of 164 Hz (Strohmayer & Keek 2017) that resides in an ultracompact X-ray binary (UCXB) with an orbital period of 38 min (Strohmayer et al. 2018; see also Hernandez Santisteban et al. 2018). Such a small orbit can only accommodate a small companion star, most likely a white dwarf that is denuded from its upper hydrogen layers through mass transfer (e.g., Nelson et al. 1986; Savonije et al. 1986). IGR J17062–6143 was discovered in 2006 (Churazov et al. 2007) and has been active ever since with a low luminosity of $L_{\text{X}} \simeq (1-5) \times 10^{35} \left(\frac{D}{5.0 \text{ kpc}}\right)^2 \text{ erg s}^{-1}$ (Ricci et al. 2008; Remillard & Levine 2008; Degenaar et al. 2012b; Keek et al. 2017; van den Eijnden et al. 2018). It was identified as an accreting neutron star low-mass X-ray binary (NS LMXB) through the X-ray burst discussed here that occurred on June 25, 2012, which was classified as a rare energetic intermediate-duration X-ray burst by Degenaar et al. (2013, 2017). A second X-ray burst was detected in March 2015 with MAXI and was followed up with XRT after 10^4 s (Keek et al. 2017). The absorption column density amounts to $N_{\text{H}} = 1.2 \times 10^{21} \text{ cm}^{-2}$ (Keek et al. 2017; van den Eijnden et al. 2018) which is the lowest in our sample.

This burst is a nice showcase for the kind of burst we present here because it is bright, long, has small interstellar absorption,

² http://www.swift.ac.uk/analysis/xrt/digest_cal.php

Table 2. Spectral fits to six down/up spectra presented in Fig. 3.

Burst id.	Exposures (s)	N_{H} (10^{21} cm^{-2})	kT_{lo} (keV)	kT_{hi} (keV)	0.7–10 keV flux ($10^{-9} \text{ erg s}^{-1} \text{ cm}^{-2}$) lo/hi	χ^2_{ν} (d.o.f.)	Chance prob.
IGR J17062–6143/2012-06-25	174.7/304.5	1.2	1.76 ± 0.04	1.52 ± 0.02	5.3(1)/7.8(1)	1.238(695)	1.7×10^{-5}
SAX J1712.6–3739/2011-09-26	158.7/25.0	15.4	2.11 ± 0.08	2.26 ± 0.08	3.1(2)/27.0(9)	1.237(247)	6.5×10^{-3}
SAX J1712.6–3739/2014-08-14	161.7/753.3	15.4	1.85 ± 0.12	1.64 ± 0.02	0.90(8)/3.58(5)	1.051(540)	2.0×10^{-1}
Swift J1734.5–3027/2013-09-01	68.9/79.9	5.7	1.69 ± 0.05	1.96 ± 0.03	5.5(2)/19.3(4)	0.919(514)	9.1×10^{-1}
IGR J18245–2452/2013-03-30	139.2/265.6	2.2	0.97 ± 0.03	1.04 ± 0.02	0.41(2)/0.73(2)	1.713(208)	6.8×10^{-10}
4U 1850–087/2014-03-10	21.4/338.0	4.8	1.64 ± 0.07	1.82 ± 0.02	7.9(5)/16.3(2)	1.700(786)	3.6×10^{-31}

Notes. For IGR J17062–6143, only data above 2 keV were fitted. N_{H} was not fitted (for literature values, see text). The last column refers to the chance probability that χ^2_{ν} is higher than the observed value.

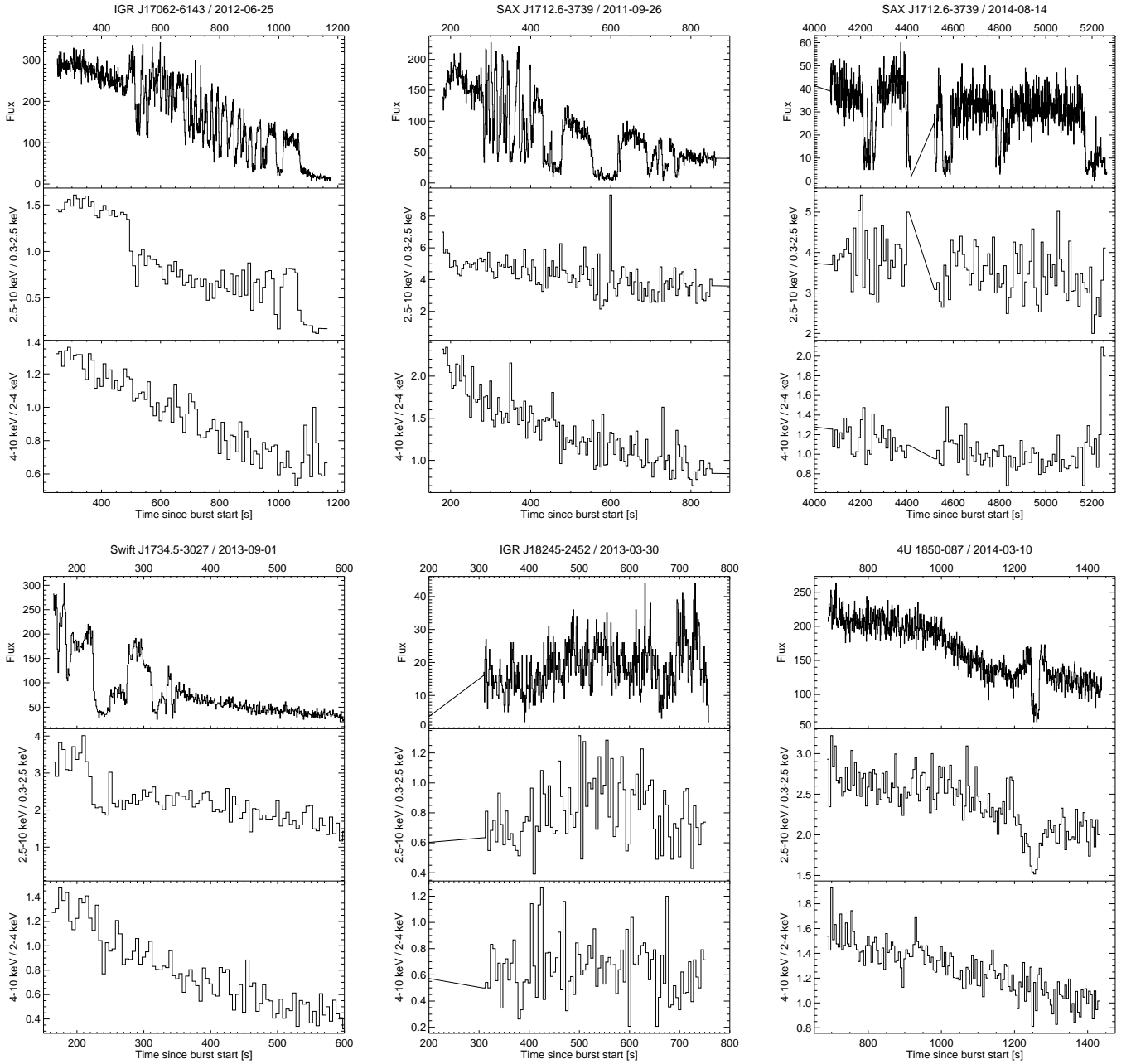


Fig. 2. Time profiles of the XRT data of the six selected bursts: of the intensity (*top panels*), the 2.5–10 keV/0.25–2.5 keV hardness ratio (*middle panels*) and the 4–10 keV/2–4 keV hardness ratio (*bottom panels*). Times are since burst onset as determined from BAT data.

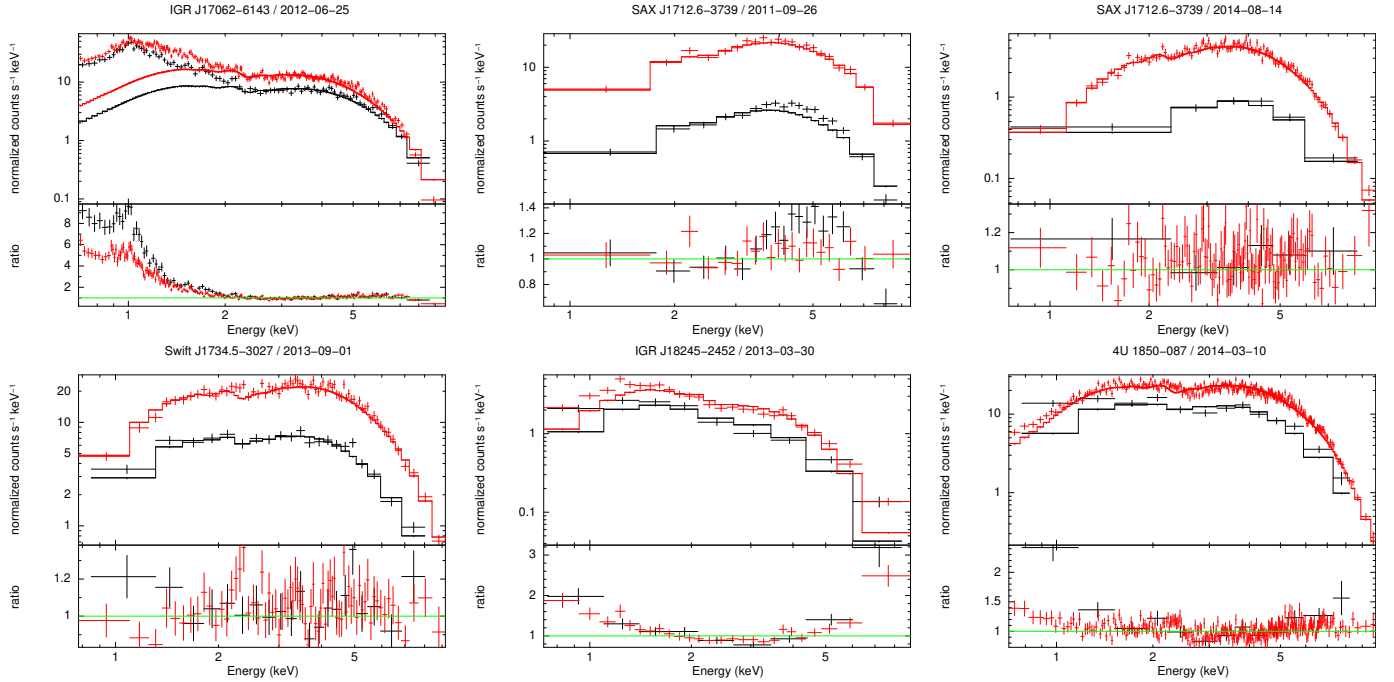


Fig. 3. Spectra of the upward and downward fluctuations for the six selected bursts. For IGR J17062–6143, only data above 2 keV were fitted. The lower panels show the ratio of the data to the applied model. Black data points are for “lo” data, red for the “hi”.

and is well covered by BAT and XRT. In the BAT light curve (Fig. 1) there are a lot of fluctuations at the start of the burst. These fluctuations are not significant, but statistical in nature because the source is off-axis in the beginning. They become smaller as *Swift* slews towards the source. The touchdown point is around 220 s after the start of the burst. The XRT data, starting at 250 s after the burst start, show a plethora of fluctuation behavior starting at around 500 s with initially fast fluctuations going up and down and later also longer dips. The dip at the end is likely a long dip, which is below the decay trend of the burst.

Keek et al. (2017) have carefully assessed the bolometric flux due to accretion and find an average of $(0.92 \pm 0.07) \times 10^{-10} \text{ erg cm}^{-2} \text{ s}^{-1}$ between 2012 and 2015. This is only 0.2% of the peak luminosity of the burst. We did not subtract the persistent emission in the spectra.

For the fluctuation spectrum we used the same model as Degenaar et al. (2013) did, except we did not fit the absorption lines and iron edges. In the fitted spectra we can clearly see that the model is incorrect for the higher energies (Fig. 3). Adding absorption lines and iron edges, as Degenaar et al. (2013) did, would improve this fit at higher energies. An interesting feature of the fluctuation spectrum is that an emission line around 1 keV is observed. There seems to be a much smaller drop in count rate between the up and down fluctuations around 1 keV. The emission line energy is in the Fe-L complex. Degenaar et al. (2013) suggests that this emission line is caused by the irradiation of relatively cold gas. By dividing the full width at half maximum (FWHM) of the emission line by the line’s energy, they derive a velocity of $\sim 0.16c$, where c is the speed of light. This velocity implies a radial distance of $\sim 8 \times 10^2 \text{ km}$ from the NS for a Keplerian orbit. Degenaar et al. (2013) also found absorption lines and edges at higher energies ($>7.5 \text{ keV}$) which we did not model. They conclude that the spectral features and the fluctuations (on a timescale of 1–10 s) imply similar radial distances from the NS, and are therefore likely caused by the same material and mechanism.

Figure 4 shows the time evolution of the parameters of the blackbody spectral model. The strongest changes in bolometric flux are attributed mostly to strong changes in the normalization of the blackbody model and not in the temperature.

4.4. Bursts from SAX J1712.6–3739

SAX J1712.6–3739 was discovered in 1999 (in 't Zand et al. 1999), and since then has always been detected whenever observed. Immediately after discovery, the source was seen to burst twice with a half-minute duration (e.g., Cocchi et al. 2001). Figure 5 shows the long-term light curve between 2004 and 2018 with a one-month resolution and a semi-week resolution. The data are from PCA Bulge Scan (Swank & Markwardt 2001) and MAXI observations (Negoro et al. 2016). The source shows wide variability between 0 and 48 mCrab on both timescales with an average flux of $9.10 \pm 0.04 \text{ mCrab}$, or about $2 \times 10^{-10} \text{ erg cm}^{-2} \text{ s}^{-1}$.

When investigating the MAXI data at the highest 1.5 h time resolution, ten burst-like features show up in almost nine years of data, when the 4–10 keV flux rises above 0.2 Crab units. Two of these show high fluxes for multiple consecutive data points suggesting intermediate-duration bursts. This is consistent with an earlier finding of an intermediate-duration burst in RXTE-ASM data from 1999 (Kuulkers 2009).

In BAT Hard X-ray Transient Monitor daily-average data (Krimm et al. 2013), the source averages 7 mCrab (15–50 keV) with an incidental excursion of up to 36 mCrab, similar to values found with INTEGRAL-IBIS (4.7 mCrab in 20–40 keV during 2003–2006; Fiocchi et al. 2008a) and *BeppoSAX* (6–32 mCrab in 1–10 keV in 1999; Cocchi et al. 2001). It is clear from these measurements that the source is persistent but wildly variable on timescales of 1 day and longer. However, it never becomes brighter than about 50 mCrab. It is noted that the BAT Monitor data recently showed a burst on May 8, 2018 (Lin & Yu 2018).

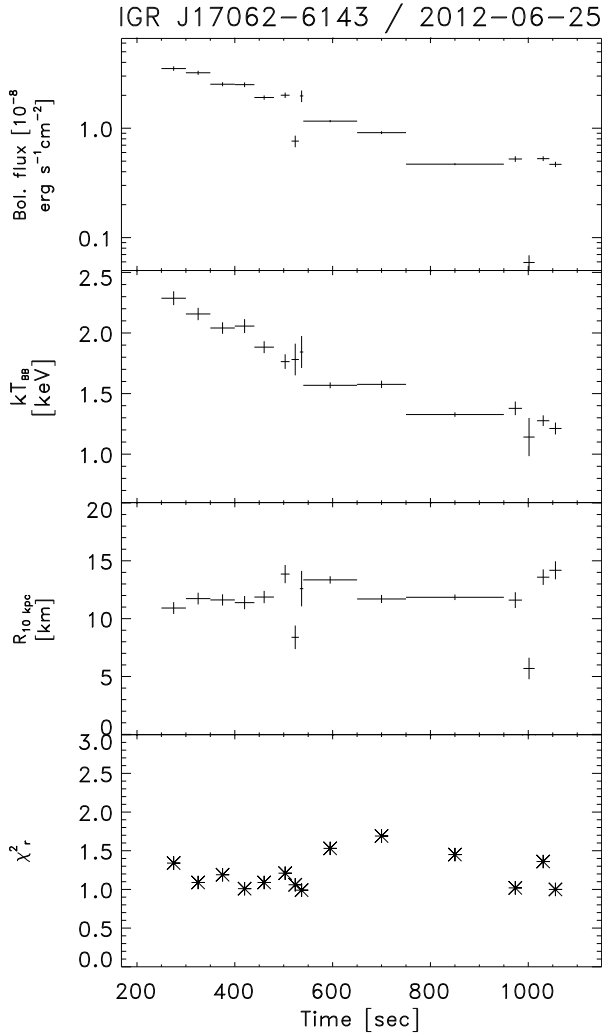


Fig. 4. IGR J17062–6143: Time-resolved spectroscopy.

SAX J1712.6–3739 is classified as a NS LMXB (Cocchi et al. 2001) which implies an average luminosity of $2 \times 10^{36} \text{ erg s}^{-1}$ or roughly 1% of Eddington. in ’t Zand et al. (2007) list this source as a candidate UCXB. Wiersema et al. (2009) find that the optical magnitudes of the likely counterpart can accommodate a UCXB nature. Revnivtsev et al. (2013) come to the same conclusion on more sensitive infrared measurements. Time-resolved optical spectroscopy of this system would be able to reveal the binary period and therefore the UCXB nature. According to Yoon et al. (2011), SAX J1712.6–3739 is to date the only known X-ray binary to display a prominent H_α bow-shock nebula and Wiersema et al. (2009) speculate that it is due to a high velocity towards the Galactic plane in a relatively dense medium and is powered by a jet. There are no published papers on bursts observed from this source with *Swift*.

We found three burst detections with BAT and XRT from SAX J1712.6–3739. The first, on July 1, 2010, is the shortest of the three and is unremarkable. The BAT rise time is 20 s. The second and third, on 2011-09-26 and 2014-08-18, are very remarkable because they are long and show strong fluctuations. This is the second source to have shown fluctuations in multiple X-ray bursts, after 2S 0918–549 (in ’t Zand et al. 2005, 2011).

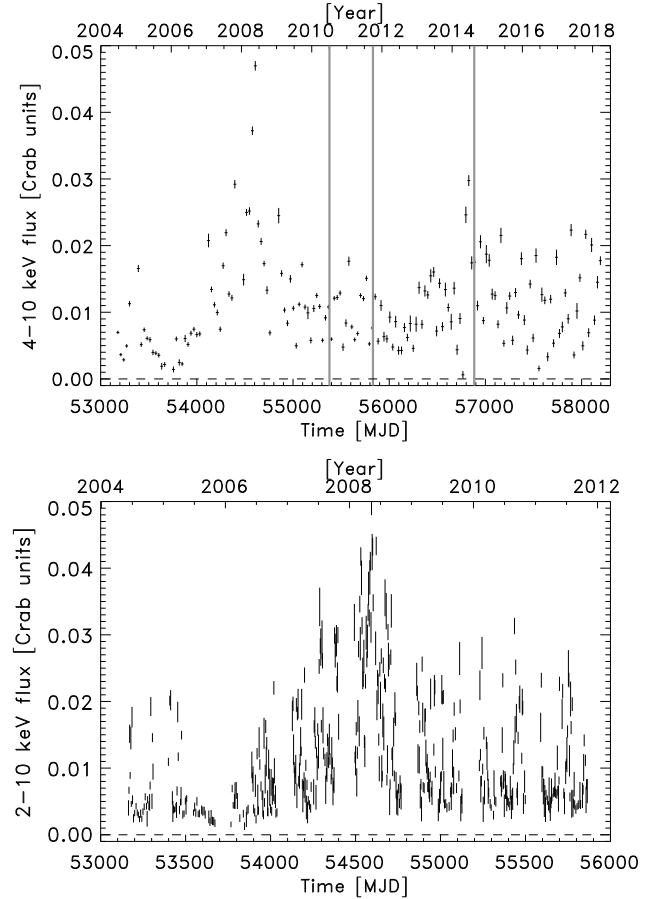


Fig. 5. Top panel: 4–10 keV light curve over 14 years for SAX J1712.6–3739 with a time resolution of 1 month. The data are from the PCA Bulge Scan program (Swank & Markwardt 2001) between 2004 and 2012, and MAXI observations between 2009 and 2018 (e.g., Negoro et al. 2016). A cross calibration has been performed for the two years that the programs overlap. Strong variability is obvious. Vertical bars indicate the times of the three bursts detected with *Swift*. Bottom panel: 2–10 keV light curve measurements with PCA over 8 years for SAX J1712.6–3739. Typically, each data point represents 1 min of data and measurements were performed twice a week. Strong variability is also obvious at this resolution.

4.4.1. Burst on September 26, 2011

In the BAT data (see Fig. 1), the end of the Eddington-limited phase is around 190 s after the start of the burst. The XRT light curve shows fast fluctuations between ~ 280 s and ~ 410 s after the burst onset with both fluctuations up as down. After the fast fluctuations have ceased, longer dips are seen. The behavior of this burst is reminiscent of that of the burst from IGR J17062–6143. The early dip at about 190 s after the burst start could be the touchdown point.

For the time-resolved spectroscopy (see Fig. 6) we fitted an absorbed blackbody. The spectra are not subtracted with the persistent flux of the source. The persistent flux measured with RXTE PCA³ on MJD 55828.100 was $32.17 \text{ counts s}^{-1} \text{ 5PCU}^{-1}$ translating to 3.217 mCrab ($7.7208 \times 10^{-11} \text{ erg cm}^{-2} \text{ s}^{-1}$), which is insignificant compared to the burst emission. The maximum burst emission of the XRT data is $4.1 \times 10^{-8} \text{ erg cm}^{-2} \text{ s}^{-1}$. After the burst on MJD 55835.219 the persistent flux was $66.95 \text{ counts s}^{-1} \text{ 5PCU}^{-1}$.

³ <https://asd.gsfc.nasa.gov/Craig.Markwardt/galscan/html/SAXJ1712.6-3739.html>

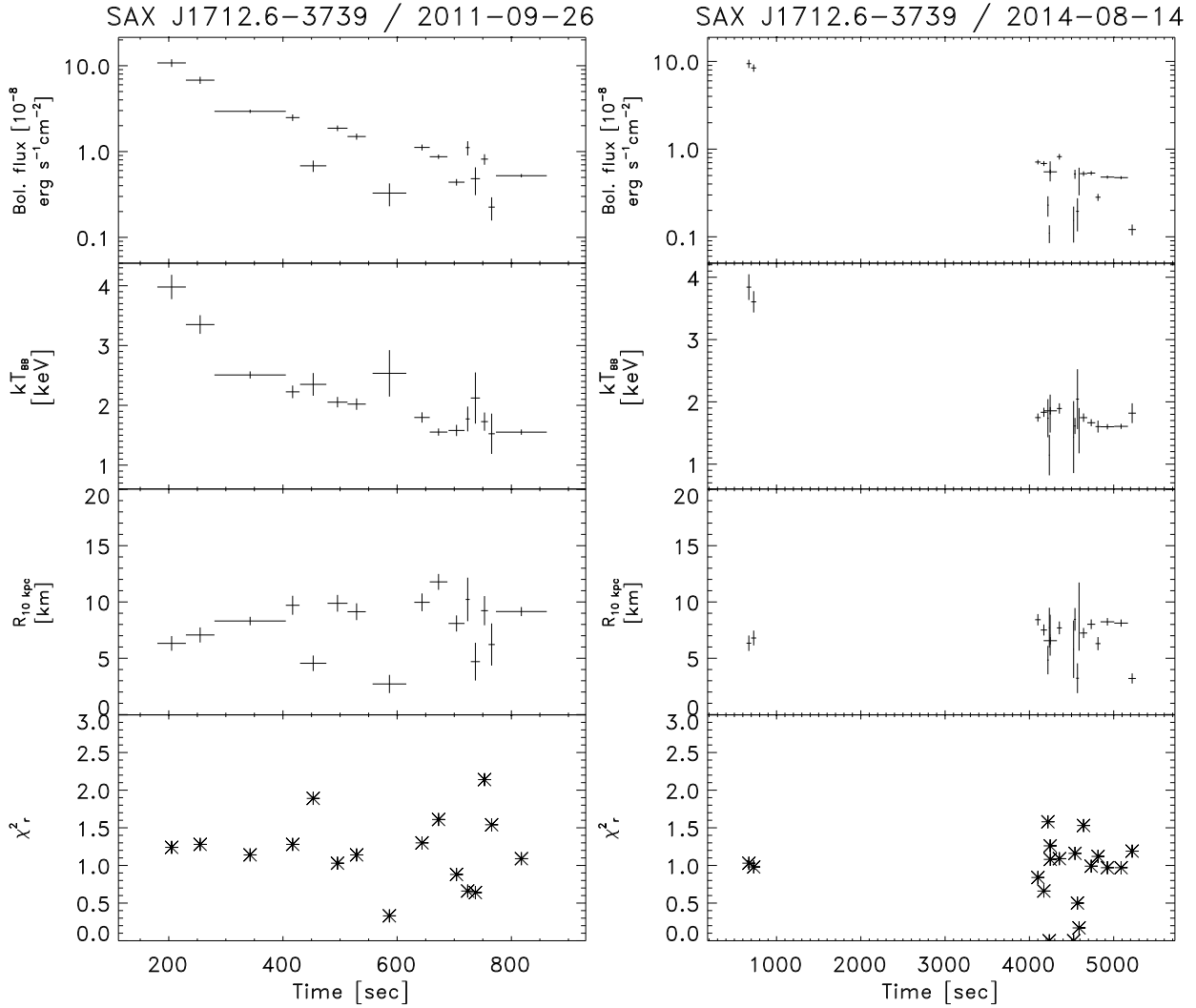


Fig. 6. SAX J1712.6–3739: Time-resolved spectroscopy of both long bursts.

For the spectrum of the fluctuations (see Fig. 3) we selected the fluctuations between ~ 340 and ~ 480 s. There is no noticeable difference between the shape of the lo and hi spectrum. The N_{H} value for this source is much higher than for the other sources. Therefore, less can be said about the lower energies of this spectrum. Figure 6 shows the time-resolved spectroscopy in the left panel. The fluctuations are represented by changes in the blackbody normalization.

4.4.2. Burst on August 18, 2014

This burst is very unusual. The mask-tagged BAT data is, unfortunately, incomplete because it is actually due to two triggers, GRB140818A and a late image trigger from SAX J1712.6–3739. The data show a short-duration (~ 15 s) X-ray burst, then a period of 40 s when no emission is detected, then a data gap of 450 s, followed by data for about 320 s until 820 s after the burst start when the flux decreases from about 100 to 70% of the peak value of the initial burst. A possible touchdown point can be identified at 540 ± 40 s. To overcome the gap in the BAT data, we investigated the rate data. The pointing of *Swift* was constant during that data gap. The result is given in Fig. 7. It shows that the BAT signal returns 50 s after the precursor ended.

The XRT data start 270 s after the burst start until 760 s and then again from 4000 to 5500 s. We verified that there is no

MAXI data during the gap. At least four eclipse-like features with 70% less flux are visible in the second data stretch of duration 20–45 s except the last one which lasts at least 90 s and is cut short by the observation end.

This is the longest burst in our sample. The e-folding time of the XRT data, simply estimated from the two observation periods, is 0.8 h. This is similar to the shortest superbursts (cf. in 't Zand et al. 2017), but those superbursts were from a high accretion-rate source. This brings us to an important question: is this a superburst or not? We discuss this in Sect. 7.2.

One could ask whether the late phase is really burst emission. We tried fitting an absorbed power law and disk blackbody for the whole period 4000–5300 s and found good fits that were, however, inconsistent with earlier findings about N_{H} . Only a single blackbody spectrum gave a consistent N_{H} value of $(15.2 \pm 0.5) \times 10^{21} \text{ cm}^{-2}$, compared to the literature value of $15.4 \times 10^{21} \text{ cm}^{-2}$. We conclude that the emission is consistent with that from the burst. The average temperature for the whole period is 2.00 ± 0.03 keV.

For comparison, we also fitted the earlier XRT spectrum and find $N_{\text{H}} = (18.7 \pm 0.6) \times 10^{21} \text{ cm}^{-2}$ and $kT = 3.84 \pm 0.09$ keV $\chi^2_{\nu} = 1.12$ ($\nu = 746$). The temperature is higher than expected even for an Eddington-limited flux (cf., Lewin et al. 1993). This is also visible in the time-resolved spectroscopy (Fig. 6), also for the other burst from SAX J1712.6–3739. We are unaware of

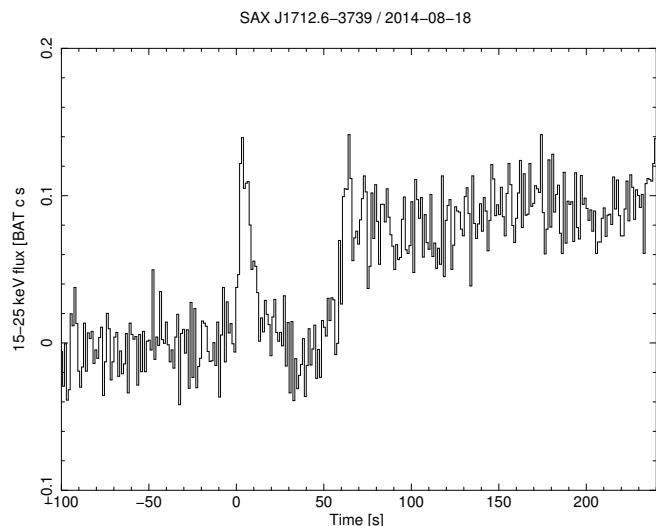


Fig. 7. BAT light curve of the third burst from SAX J1712.6–3739, reconstructed from rate meter data in 15–25 keV (pre-burst flux subtracted between –40 and 0 s from burst start and normalized to projected detector area as seen from source). During this data stretch BAT had a fixed pointing.

such high-temperature measurements in other X-ray bursts and believe it points to a special circumstance in SAX J1712.6–3739. It may be related to increased levels of the persistent flux as is often seen, particularly in PRE bursts (in ’t Zand et al. 2013; Worpel et al. 2013), but it is not possible to determine with these data given the lack of pre-burst XRT data.

4.5. Burst from Swift J1734.5-3027

Swift J1734.5–3027 is a NS LMXB transient that was discovered with *Swift* through the burst on September 1, 2013, discussed here (Malesani et al. 2013). The transient was active in November 2010, May 2013, and September–October 2013 (Negoro et al. 2016; Bozzo et al. 2015) at levels of ~ 10 mCrab, which is two orders of magnitude smaller than the burst peak. The low peak luminosity may indicate an UCXB origin (Heinke et al. 2015). An XMM observation (Bozzo et al. 2015) exhibited cold interstellar absorption at a level of $N_{\text{H}} = (5.7 \pm 0.8) \times 10^{21} \text{ cm}^{-2}$. So far, only the one burst was detected, testifying that the accretion rate never reaches values in excess of about 1% of Eddington.

The BAT light curve shows a fairly long rise time of ≈ 50 s. Bozzo et al. (2015) cannot firmly assess whether the burst actually underwent PRE, but this light curve certainly suggests that it did. The XRT continuous measurement of the burst lasted for 1700 s. Some additional snapshots were taken 3000 s later. The XRT data start with two short dips of about 50% and 2 s and 5 s duration. Then a 50 s long dip of depth 80% is seen with a step upward of 20% halfway through the dip. Two final dips of 20 s and 6 s follow of about 80% depth. Bozzo et al. (2015) does not discuss the dips.

For the time-resolved spectroscopy, see Fig. 8. It shows that the dips are completely attributable to a decrease in the blackbody normalization.

4.6. Burst from IGR J18245-2452

Since the XRT light curve does not show a decreasing trend, we checked whether this emission is due to the X-ray event

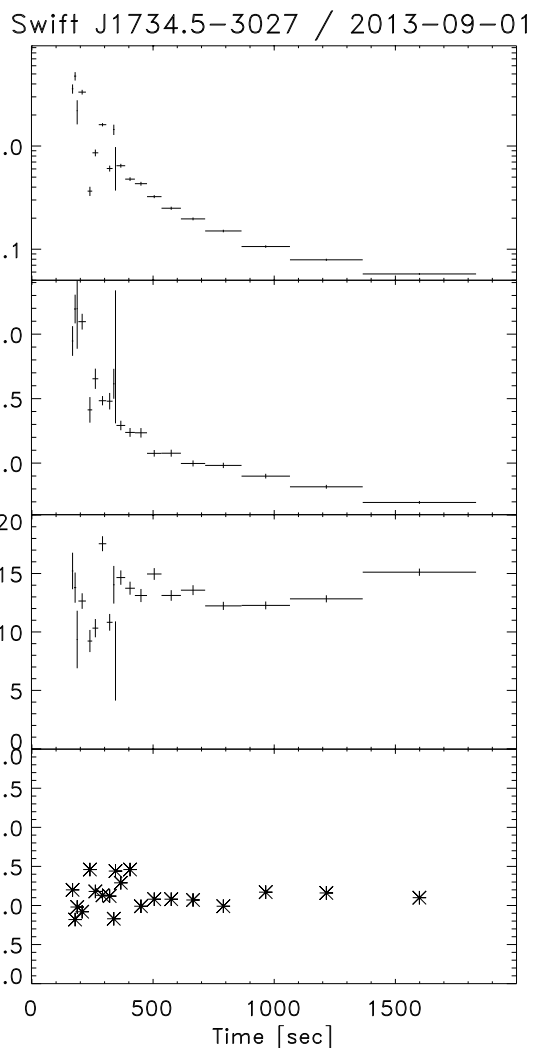


Fig. 8. Swift J1734.5–3027: Time-resolved spectroscopy.

detected with BAT. First, we checked whether the spectrum is best described by a blackbody. We tested the following prescriptions and found the related χ_r^2 values: a power law ($\chi_r^2 = 0.95$ with $\nu = 209$, $\Gamma = 1.22 \pm 0.05$, $N_{\text{H}} = (0.39 \pm 0.04) \times 10^{22} \text{ cm}^{-2}$), a Comptonized spectrum (comptt in XSPEC; $\chi_r^2 = 0.96$ with $\nu = 207$, $N_{\text{H}} = (0.40 \pm 0.13) \times 10^{22} \text{ cm}^{-2}$), a disk blackbody ($\chi_r^2 = 0.86$ with $\nu = 209$, $kT_{\text{in}} = 2.93 \pm 0.18 \text{ keV}$, $N_{\text{H}} = (0.23 \pm 0.03) \times 10^{22} \text{ cm}^{-2}$) and a blackbody ($\chi_r^2 = 1.24$ with $\nu = 209$, $kT = 1.11 \pm 0.02$, $N_{\text{H}} < 0.37 \times 10^{22} \text{ cm}^{-2}$). Although the data do not really allow to make a distinction between models, a blackbody is the least probable. IGR J18245–2452 is located in the globular cluster M28 with a reddening of $E(B - V) = 0.4$ (Harris 1996), implying $N_{\text{H}} = 0.22 \times 10^{22} \text{ cm}^{-2}$ which is consistent with the value found for the disk blackbody and simple blackbody. The absorbed 0.7–10 keV flux is $(8.6 \pm 0.3) \times 10^{-10} \text{ erg s}^{-1} \text{ cm}^{-2}$.

Figure 9 shows the time-resolved spectroscopy of the XRT data for this event. It shows a general cooling trend, although only after the peak at 400 s at a rather low temperature which is unexpected for an X-ray burst.

IGR J18245–2452 is a transient LMXB which was detected so far only once. The outburst lasted from March 26 to April 17, 2013 (De Falco et al. 2017). It was highly variable with a peak bolometric flux of $3 \times 10^{-8} \text{ erg s}^{-1} \text{ cm}^{-2}$. De Falco et al. (2017) report 3 X-ray bursts, one of which with *Swift* on

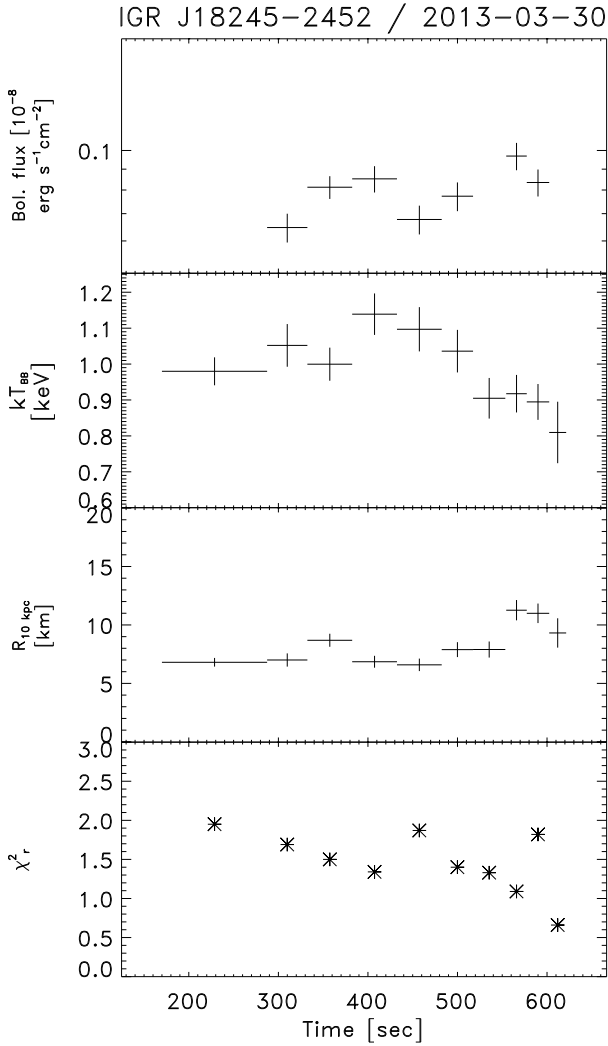


Fig. 9. IGR J18245–2452: Time-resolved spectroscopy.

2013-04-07 (Papitto et al. 2013a; see also Table A.2). However, there may have been a further detection with ASCA in 1995 (Gotthelf & Kulkarni 1997). IGR J18245–2452 is a transitional millisecond pulsar (Papitto et al. 2013b) with a very hard spectrum (Parikh et al. 2017) and extreme variability (Wijnands et al. 2017). The orbital period is 11.0 h (Papitto et al. 2013a), so this is not a UCXB.

We here report a fourth burst-like event which was actually the first in the outburst, 4.6 d after the outburst onset. De Falco et al. (2017) study the broad-band persistent spectrum when the flux is $4 \times 10^{-10} \text{ erg s}^{-1} \text{ cm}^{-2}$ and find that a power-law fit yields a hard photon index $\Gamma = 1.4$ which is similar to what we find in the aftermath in XRT data of the burst detected with BAT. They find $N_{\text{H}} = 0.24 \times 10^{22} \text{ cm}^{-2}$ which is also consistent. This supports the notion that the emission in our XRT data is not due to the burst and likely an expression of the strong variability inferred by Wijnands et al. (2017). We, therefore, refrain from further discussing this event.

4.7. Burst from 4U 1850-087

4U 1850–087 is an ultracompact X-ray binary (UCXB) with a tentative orbital period of 20.6 min (Homer et al. 1996). 4U 1850–087 is located in the globular cluster NGC 6712. From XMM-Newton observations, Sidoli et al. (2005) find

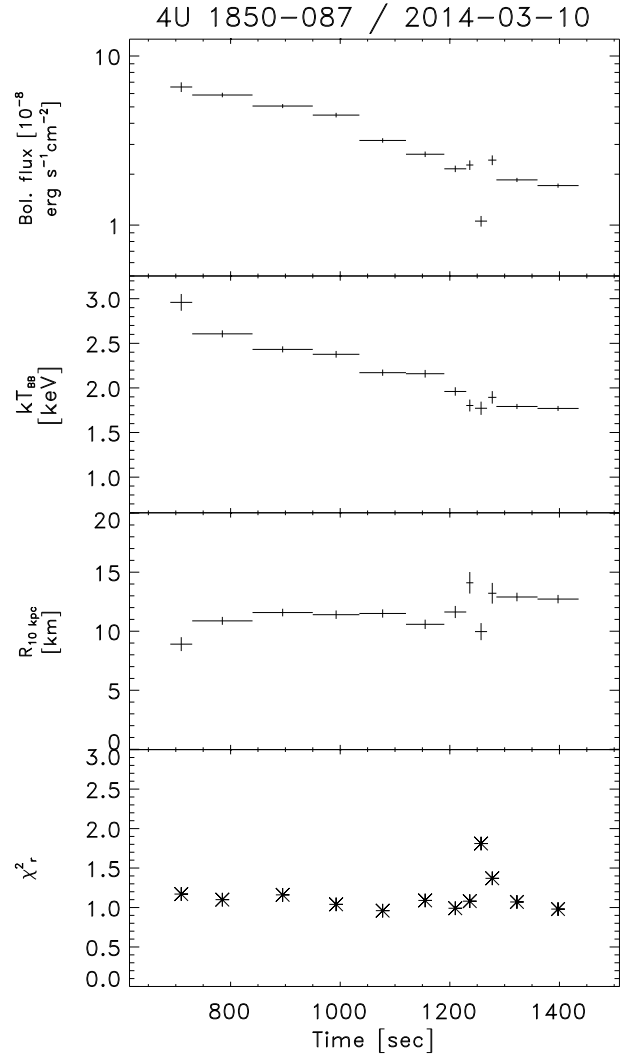


Fig. 10. 4U 1850–087: Time-resolved spectroscopy.

$N_{\text{H}} = (4\text{--}6.3) \times 10^{21} \text{ cm}^{-2}$ with evidence for extra absorption in the line of sight, since the best-fit total N_{H} is always significantly higher than the optically derived value in the direction of the host globular cluster of $(1.8 \pm 0.2) \times 10^{21} \text{ cm}^{-2}$. Therefore, the intrinsic absorption ranges from 2 to $4.5 \times 10^{21} \text{ cm}^{-2}$.

On March 10, 2014, 4U 1850–087 triggered *Swift* following an image trigger over 392 s. After BAT completed the analysis in 26 s, the observatory slewed to the source in 69 s. The first WT mode data is available 691 s after the start of the burst (in 't Zand et al. 2014b). The measurement lasted around 760 s. In the XRT light curve (see Fig. 2) we see the decay of a thermonuclear X-ray burst. A dip of ~ 20 s long is clearly visible, which is ~ 660 s after the touchdown. Just before and after this dip, the count rate is above the overall decay trend.

For the time-resolved spectroscopy, we fitted the spectra with an absorbed blackbody (see Fig. 10). The XRT data do not show evidence for PRE, as expected given that the touch down point in BAT data is prior to the XRT data. The dip is mostly due to a change in the normalization of the blackbody and not to one in blackbody temperature. An analogous remark can be made about the increased fluxes before and after the dip. The spectrum of the dip (Fig. 3) shows a small peak around 1 keV, although less clear than in IGR J17062–6143.

The burst has a touchdown point which is about 550 s after the burst onset according to BAT data. The implied duration of the Eddington-limited phase rivals with the bursts from SLX 1735–269 and the third burst from SAX J1712.6–3739 and is only superseded by the 1400 s seen in a superburst from 4U 1820–30 (Strohmayer & Brown 2002).

The persistent emission of 4U 1850–087 as measured with MAXI from 56 600 to 56 730 MJD stays below approximately $0.02 \text{ counts cm}^{-2} \text{ s}^{-1}$ in both the 2–4 keV and 4–10 keV energy bands, except for the days around the bursts when on average the count rate was $\sim 0.01 \text{ counts cm}^{-2} \text{ s}^{-1}$. Using the WebPIMMS⁴ tool we estimate the persistent flux (2.0–4.0 keV), which is $\sim 10^{-10} \text{ erg cm}^{-2} \text{ s}^{-1}$ for a power-law index of 2. The bolometric flux may be a factor of ~ 2 larger. Since we did not model the persistent spectrum we assumed the power-law index to be 2. The persistent bolometric flux should therefore be taken with a large uncertainty of 50%. The persistent emission is, however, much smaller than the burst emission which was $5.0 \times 10^{-8} \text{ erg cm}^{-2} \text{ s}^{-1}$ at the start of the XRT data. The peak bolometric flux might be a bit higher. We did not subtract the persistent emission in the spectra.

5. Literature bursts

Nine literature cases are known (eight are listed in Degenaar et al. 2018; an additional case is from A1246–58). We provide here some details of seven of these cases that are not among the *Swift* cases. Light curves are provided in Fig. 11 and details in Tables 3–5.

5.1. 2S 0918–549

2S 0918–549 is a very likely UCXB (Juett & Chakrabarty 2003; in 't Zand et al. 2007) with a tentative orbital period of 17.4 min (Zhong & Wang 2011). Three bursts were detected with the WFC (in 't Zand et al. 2005), one of which was much longer than the others, lasting over 2500 s. The first 1000 s of this long burst are displayed in Fig. 11. The long burst showed a strong photospheric radius expansion. There were two data drop outs: from 165 to 180 s and from 350 to 354 s. After ~ 2 minutes a short period of strong fluctuations is observed. After these fluctuations a long dip starts quickly and then rises in ~ 70 s back to the decay trend of the burst.

Five X-ray bursts were detected with RXTE-PCA (in 't Zand et al. 2011). The last one (on February 8, 2008) is at least seven times longer than the others. This burst (see Fig. 11) has a very short precursor of 40 ms (see also in 't Zand et al. 2014c) with the main burst starting 1.2 s later. This burst is Eddington limited and has PRE. The interesting feature of this burst is the strong fluctuation starting 122 s after burst onset and lasting 66 s.

5.2. A 1246–58

A 1246–58 is a UCXB candidate (Bassa et al. 2006). in 't Zand et al. (2008) investigated the UCXB nature of A 1246–58 further and reported four X-ray bursts, detected with the *BeppoSAX* WFC. All four bursts are Eddington limited, one of which (Fig. 11) shows two deep dips in the tail lasting tens of seconds. The dips are between 85 and 150 s while the PRE phase lasts until 55 s after burst onset. The burst exhibits superexpansion.

⁴ <http://heasarc.gsfc.nasa.gov/cgi-bin/Tools/w3pimms/w3pimms.pl>

5.3. SLX 1735–269

SLX 1735–269 (Skinner et al. 1987) is a UCXB candidate (in 't Zand et al. 2007). During observations of the Galactic center region in 2003, INTEGRAL detected six X-ray bursts (Molkov et al. 2005). One of them (see Fig. 11) lasted over 2000 s and starts with a 2 s precursor. Eight seconds after the precursor, the main burst started. This burst has an Eddington-limited phase of about 450 s. This burst also has superexpansion based on the fact that a precursor is seen. Molkov et al. (2005) conclude that the long burst was most likely a result of the unstable burning of hydrogen and helium, but we contend that this looks like an intermediate-duration burst. The burst has many fluctuations, both up and down in count rate. These fluctuations start before the touchdown (~ 500 s), although the early fluctuations should be considered with caution since they were measured in a non-standard observation mode (Chenevez, priv. comm.).

5.4. GRS 1741.9–2853

GRS 1741.9–2853 is a transient LMXB with peak accretion luminosities $< 10^{37} \text{ erg s}^{-1}$ (Muno et al. 2003; Trap et al. 2009; Degenaar et al. 2015). Whether GRS 1741.9–2853 is a UCXB is an unsettled matter. None of the previously detected X-ray bursts from this source (Muno et al. 2003; Galloway et al. 2008; Trap et al. 2009) clearly resolves an rp-component in the light curve, which would identify hydrogen and suggest a non-UCXB nature (e.g., in 't Zand et al. 2017). The burst series and repetitive buildup of burst ignition conditions indicates that pure helium is burned during the bursts (Trap et al. 2009). The sole presence of pure helium bursts at apparently low accretion rates would be typical of UCXBs.

In August 2013, NuSTAR detected an intermediate-duration PRE burst lasting at least 800 s and with a fairly short exponential decay time of 21 s (Barrière et al. 2015). The LMXB was on the rise of a transient outburst and was at a persistent bolometric luminosity about 445 times smaller than the burst peak luminosity. The burst has two periods of fluctuations: up and down fluctuations from 48 to 65 s on a timescale of a few seconds and with a dip between 75 and 95 s. The PRE touchdown point is at about 30 s.

5.5. 4U 1820–30

4U 1820–30 is the prototypical UCXB with the shortest orbital period of 11 min (Stella et al. 1987). In 1999 it exhibited a superburst in RXTE/PCA observations (Strohmayer & Brown 2002). These data show fluctuations happening (in 't Zand et al. 2011) on timescales between 1 and 10 s and amplitudes up to 30% between 3365 and 7200 s with a PRE phase until 1400 s. No eclipse-like features were seen.

5.6. M15 X-2

This burst was detected in 1988 from M15 X-2 with the Large Area Counter on the Japanese X-ray observatory Ginga (van Paradijs et al. 1990). M15 X-2 is a UCXB with an orbital period of 22.6 min in the globular cluster M15 (Dieball et al. 2005). The burst is an intermediate-duration burst visible for 160 s. It has superexpansion and a PRE stage lasting about 95 s. During the post-PRE stages the general e-folding decay time is about 60 s. The source shows fluctuations on a typical timescale of 1 s between 127 and 152 s. No long timescale dips have been detected, but that could be because the observation stopped prematurely.

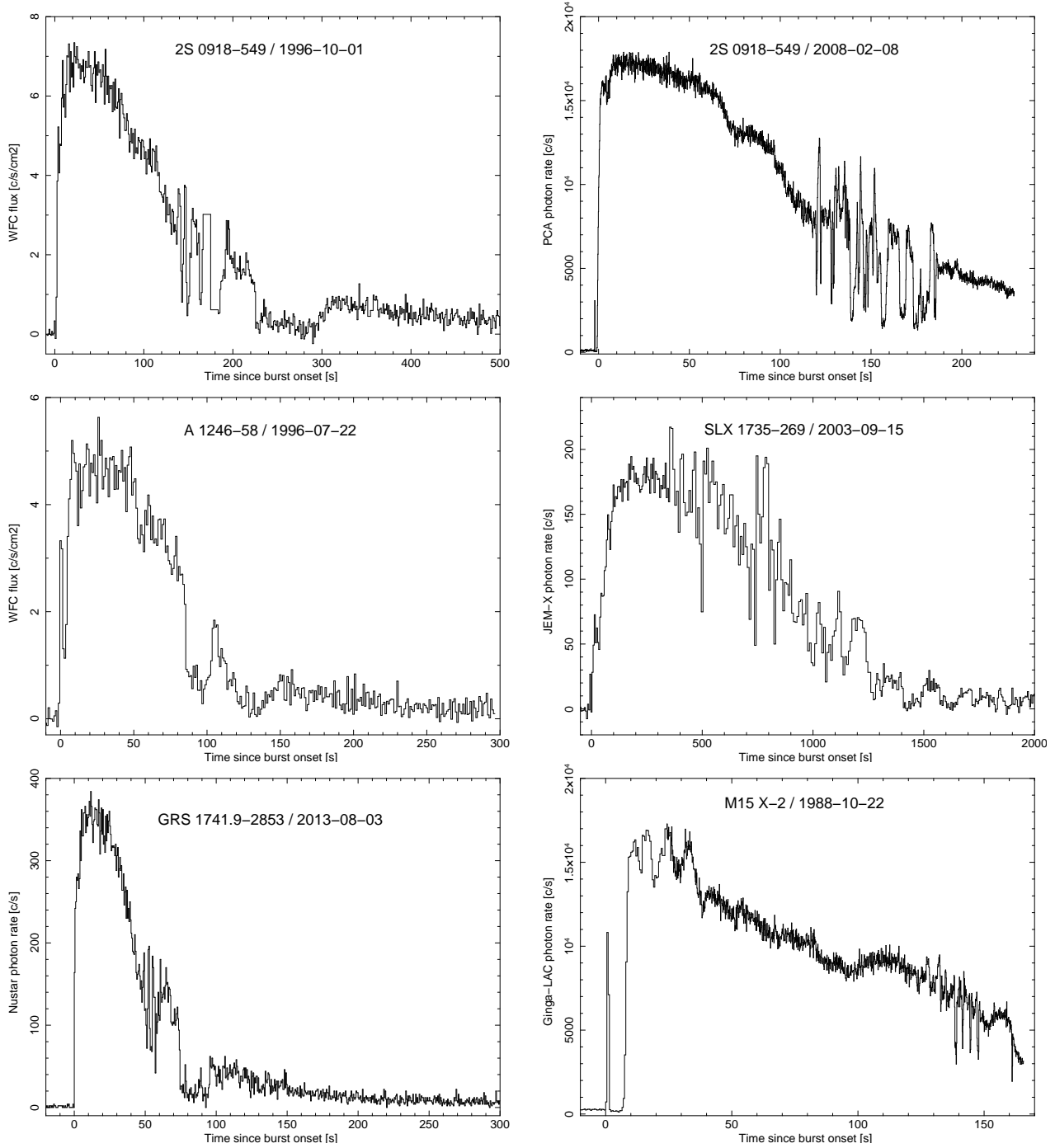


Fig. 11. Light curves of literature bursts with fluctuations.

6. Comparative analysis

6.1. Data

Light curves of all bursts, except the superburst of 4U 1820–30, are provided in Figs. 2 and 11. Table 3 contains general information about the ten sources including the type of binary, the hydrogen absorption column density, the type of accretion (persistent or transient), and references. Table 4 presents the parameters describing each burst, such as the e-folding decay time and the timing properties of the fluctuations. All decay times are longer than ~ 100 s, except for the bursts from 1A 1246–588, which is 55 s, and GRS 1741.9–2853, which is 46 s. The $t_{5\%}$ duration is often constrained by a lower limit alone because the data are

incomplete. However, we note that all are consistent with those of intermediate-duration bursts (>150 s).

For the bursts detected with *Swift*, we determined the touchdown time by examining the peaks in the BAT light curves. Unless the touchdown time was reported in the reference of the literature burst, the touchdown time was estimated from the peak in the plot of the blackbody temperature (kT , to be more exact). We also determined the timing properties of the fast fluctuations seen in the light curves (see Figs. 2 and 11). The last column of this table presents how much the bolometric flux has dropped, as a percentage of the peak flux, at the start of the fluctuations. For the calculation of the drop in bolometric flux we used the HEASARC WebPIMMS tool. This tool allows

Table 3. General properties of sources and data coverage of fluctuating bursts (literature bursts below the dividing line).

Burst	Object	Ultracompact?	$N_{\text{H}}/10^{22}$	P/T	Date	Instrument	Data coverage (s)
1	IGR J17062–6143	Confirmed ^[3,4,13]	0.12 ^[17]	P ^[4]	2012-06-25	<i>Swift</i> /BAT+XRT	–89/+1321
2	SAX J1712.6–3739	Candidate ^{[1],[5]}	1.54 ^[6]	P ^[1]	2011-09-26	<i>Swift</i> /BAT+XRT	–119/+924 ^a
3	SAX J1712.6–3739	“	“	“	2014-08-18	<i>Swift</i> /BAT+XRT	0/+5200
4	Swift J1734.5–3027	Possibly	0.57	T ^[2]	2013-09-01	<i>Swift</i> /BAT+XRT	–215/+1691 ^b
5	4U 1850–087	Confirmed ^[1]	0.48 ^[9]	P ^[1]	2014-03-10	<i>Swift</i> /BAT+XRT	–39/+1444
6	2S 0918–549	Semi-confirmed ^[10]	0.35 ^[9]	P ^[1]	1996-10-01	<i>BeppoSAX</i> /WFC	–13/+1002
7	2S 0918–549	“	“	“	2008-02-08	RXTE/PCA	–768/+315
8	A 1246–58	Candidate ^[1]	0.50 ^[8]	P ^[1]	1996-07-22	<i>BeppoSAX</i> /WFC	–31/+199
9	SLX 1735–269	Candidate ^[1]	1.50 ^[7]	P ^[1]	2003-09-15	INTEGRAL/JEM-X	–1200/+2235
10	GRS 1741.9–2853	Probably not ^[11,14]	11.4 ^[11,14]	T	2013-08-03	NuSTAR	<–100/+800
11	4U 1820–30	Confirmed ^[15]	0.16	P	1999-09-09	RXTE/PCA	–152/+9200
12	M15 X-2	Confirmed ^[16]	0.07 ^[12]	P	1988-10-20	Ginga/LAC	<–100/+160

Notes. All times are in seconds after the start of the burst, unless noted otherwise. ^(a)This data coverage is continuous. The rest of the XRT data beyond 5713 s are short intervals with count rates below 9.5 c s^{-1} ; ^(b)this data coverage is continuous. The rest of the XRT data beyond 5007 s are short intervals with count rates below 30 c s^{-1} .

References. [1]: [in ’t Zand et al. \(2007\)](#), [2]: [Bozzo et al. \(2015\)](#), [3]: [Keek et al. \(2017\)](#), [Hernandez Santisteban et al. \(2018\)](#), [4]: [Degenaar et al. \(2013, 2017\)](#), [5]: [Wiersema et al. \(2009\)](#), [6]: [Fiocchi et al. \(2008b\)](#), [7]: [David et al. \(1997\)](#), [8]: [in ’t Zand et al. \(2008\)](#), [9]: [Sidoli et al. \(2005\)](#), [10]: [Zhong & Wang \(2011\)](#), [11]: [Barrière et al. \(2015\)](#), [12]: [van Paradijs et al. \(1990\)](#), [13]: [Strohmayer et al. \(2018\)](#), [14]: [Trap et al. \(2009\)](#), [15]: [Stella et al. \(1987\)](#), [16]: [Dieball et al. \(2005\)](#), and [17]: [van den Eijnden et al. \(2018\)](#).

Table 4. Fast fluctuation properties.

Burst	Object	E-folding decay time (s)	$t_{5\%}$ (s)	Touch down time (s)	Start time fluct. (after touchdown) (s)	Start time fluct. (Eddington phase duration)	End time fluct. (s)	Time-scale fluct. (s)	Drop bol. flux (%) until fluct.
1	IGR J17062–6143	743	1300	220	540(240)	$\frac{540}{300} = 1.80$	1125	19	78
2	SAX J1712.6–3739	449	1050	190	330(110)	$\frac{330}{200} = 1.38$	480	11	74
3	SAX J1712.6–3739	3000	6000	500	–	–	–	–	–
4	Swift J1734.5–3027	174	600	75	–	–	210	20	71
5	4U 1850–087	1017 ^a	1400	480	–	–	–	–	–
6	2S 0918–549	130	420	85 ^[3]	135(50)	$\frac{135}{85} = 1.59$	195	9	68
7	2S 0918–549	97	500	77 ^[4]	122(45) ^[1,3]	$\frac{122}{77} = 1.58$	188	6	75
8	A 1246–58	55	200	55 ^[2]	–	–	–	–	–
9	SLX 1735–269	425	2200	420 ^[1]	380(–40)	$\frac{450}{420} = 1.07$	1230	49	0
10	GRS 1741.9–2853	46	240	30	48(18)	$\frac{48}{30} = 1.6$	65	60	25
11	4U 1820–30	3950	>9200	1400	2640	$\frac{2640}{1400} = 1.9$	7170	3	50
12	M15 X-2	98	>165	95	125(95)	$\frac{125}{95} = 1.3$	147	70	55

Notes. All times are in seconds after the start of the burst, unless noted otherwise. ^(a)From ~ 20 s to ~ 300 s the light curve is flattened. If the exponential function is fitted to the light curve after this flat phase, the e-folding time decreases significantly to 130.37 ± 31.35 s. More information in Sect. 4.7.

References. [1]: [Molkov et al. \(2005\)](#), [2]: [in ’t Zand et al. \(2008\)](#), [3]: [in ’t Zand et al. \(2005\)](#), and [4]: [in ’t Zand et al. \(2011\)](#).

us to calculate count rates from fluxes or vice versa for different satellites. As input for the five *Swift* bursts we use the BAT peak count rate. The input energy range of the BAT is 15–150 keV and as output energy range we use 0.01–40 keV as bolometric flux for a blackbody. The tool then calculates the flux of a blackbody with a peak temperature. The accuracy of these calculations is estimated to be on the order of ten percent.

In the last table (Table 5), we present timing properties of the eclipse-like features called “dips”. When more than one dip is seen in the light curve, the dip duration column presents the average duration of the dips seen.

6.2. Findings

Of the ten sources, eight are UCXBs (or candidates), which implies a small orbit and hydrogen-deficient accretion. The nature of the two remaining sources (Swift J1734.5–3027 and GRS 1741.9–2853) is undetermined, but a UCXB nature is not excluded.

We distinguish two general types of variability: fast fluctuations above and below the interpolated burst decay trend, and slow dips or partial eclipse-like features. The fast fluctuations have a typical timescale of a few to several tens of seconds (see Table 4) and an amplitude of $\sim 70\%$ above or below the average trend. In the eclipse-like features the flux only goes down,

Table 5. Dip properties.

Burst	Object	Start dips (s)	End dips (s)	Ingress & egress time (s)	Dip duration(s)	Decay during dip?
1	IGR J17062–6143	1125	Beyond data coverage?	3 & 3	≥107	Yes
2	SAX J1712.6–3739	480	840	8 & 3 (or 9)	60	Yes
3	SAX J1712.6–3739			8 & 3 (or 9)	200	No
4	Swift J1734.5–3027	210	320	3 & 3	38	No
5	4U 1850–087	1020 or 1240	Beyond data or 1270	1 & 2	30	Yes
6	2S 0918–549	220	310	2 & 70	90	Yes
7	2S 0918–549	–	–	–	–	–
8	A 1246–58	85	150	2 & 4; 4 & 8	30	Yes
9	SLX 1735–269	1230	1652	5 & 10	80	No
10	GRS 1741.9–2853	72	>165	5 & 5	5	Yes
11	4U 1820–30	–	–	–	–	–
12	M15 X-2	145	95	2 & 2	23	Yes

Notes. All times are in seconds after the start of the burst, unless noted otherwise. When multiple dips are seen, an average duration of the dips is given.

sometimes by as much as ~90%. In most cases the burst decay remains visible during the eclipse (see Table 5). This is not the case for the burst from Swift J1734.5–3027 where halfway through the two dips the flux suddenly rises to a level between the first part of the dip and the out-of-dip decay (see Fig. 2). Seven of the 12 bursts discussed here have both types of variabilities, 2 only have eclipse-like features and 3 only have only fast fluctuations. The lack of any of the two types of variability may be due to lack of full burst coverage and it could well be true that all bursts exhibit both kinds of variability.

The variability always occurs after the PRE-phase (i.e., after the touchdown) except perhaps for SLX 1735–269 where the variability seems to occur ~40 s before the touchdown point, but this measurement may be affected by instrumental behavior (the observational mode was not standard; Chenevez, priv. comm.). Disregarding SLX 1735–269, the fluctuations start at 1.5 ± 0.4 times the PRE duration for the bursts for which this ratio could be determined. The fluctuations and dips are visible in the hardness ratio of 2.5–10/0.3–2.5 keV for all the burst, except for the one from SAX J1712.6–3739 (probably because N_{H} is relatively high), but are never seen in the hardness ratio of 4.0–10/2.0–4.0 keV. This suggests that the fluctuations are not completely achromatic as earlier suggested by in 't Zand et al. (2011), but only above about 2 keV, ergo above the spectral regions where most line and edge features are situated.

The long-known and widely studied sources 4U 1850–087, 2S 0918–549, A 1246–58, SAX J1712.6–3739, SLX 1735–269, and GRS 1741.9–2853 are not known to be dippers or eclipsers (in 't Zand et al. 2007; Trap et al. 2009). Dips are due to a bulge of the accretion disk, where the accretion stream impacts the accretion disk. Eclipses are due to the donor star. Both features periodically or quasi-periodically obscure the line of sight to the inner X-ray bright part of the disk. Dips and/or eclipses from the sources Swift J1734.5–3027 and IGR J17062–6143 have also not been seen, although it should be noted that they have not been observed much yet. This indicates that the sources are all viewed from an inclination angle of less than 60° (Horne 1985).

The bursts are all intermediate-duration bursts, lasting longer than normal X-ray bursts (tens of seconds) but shorter than superbursts (several hours, see also Sect. 7.2). It is tempting to attribute the fluctuations that we see to a selection effect because it is, of course, more likely to see fluctuations in longer bursts than in shorter ones. However, short bursts have been seen ~100

times as often as intermediate-duration bursts, which counteracts this selection effect.

The bursts all have photospheric radius expansion and SLX 1735–269 (Molkov et al. 2005), 2S 0918–549 (in 't Zand et al. 2011), and A 1246–58 (in 't Zand et al. 2008) show superexpansion, reaching an emission radius of over 1000 km. The first burst from 2S 0918–549 (in 't Zand et al. 2005) does not have superexpansion unless the precursor lasts shorter than ~0.1 s as the second burst does, when it would not be detectable. The burst from GRS 1741.9–2853 for certain has no superexpansion (Barrière et al. 2015). For the five bursts detected with *Swift*, no XRT data are available for the first 100 s. Therefore, it is difficult to check whether superexpansion happened. Degenaar et al. (2013) suggest that it is plausible that superexpansion happened in the burst from IGR J17062–6143. The BAT data of the last burst from SAX J1712.60–3739 show a clear long (15 s) precursor and an unprecedented long (50 s) intermission to the main burst phase. The 2–10 keV X-ray flux may, however, remain above zero.

We cannot exclude that the fluctuations are more likely to be related to the intermediate-duration nature of the bursts in combination with long PRE phases than with the UCXB nature of the hosts. The reason for the dominance UCXBs may well be due to intermediate-duration bursts occurring predominantly, but not exclusively, on UCXBs.

Comparing the spectra from 4U 1850–087 (Fig. 3) and IGR J17062–6143 (Fig. 3), we see that both have an interesting feature below 2 keV. Although we are looking at two different parts of the burst (at the dip for 4U 1850–087 and at the fluctuations for IGR J17062–6143), they both have excesses there. In IGR J17062–6143 it is a broad emission line, while in 4U 1850–087 it is a broader excess. Logically, the count rate is lower for the downward fluctuations than the count rate for the upward fluctuations, but around 1 keV the difference in count rate is much smaller. In the case of 4U 1850–087 the count rate is approximately equal around 1 keV for both the dip (~30 s) and the times around the dip (from 30 s before the dip start and from the end of the dip to 30 s after the dip). A small peak in the downward fluctuations of Swift J1734.5–3027 (Fig. 3) is also visible around ~1.4 keV. The model in that spectrum is also underestimated in the 1 keV area as is the case with 4U 1850–087 and IGR J17062–6143. A 1 keV emission feature is most prominent in the burst from IGR J17062–6143. SAX J1712.6–3739 has a N_{H} -value which is much higher than for the other three bursts

which makes it difficult to detect any feature in the spectrum below 2 keV (see Fig. 3).

7. Discussion

7.1. Fluctuations

in 't Zand et al. (2011) interpret burst fluctuations on the basis of six bursts. The sample has now doubled, but most observational parameters of this phenomenon have not changed, in particular the amplitude, timescale, and delay time with respect to the Eddington-limited phase. One change is that the fluctuations appear achromatic above 2 keV, but not at lower energies. There sometimes is an excess, which in one case is consistent with a broad emission line. Another change is that the UCXB nature may not be a prerequisite for fluctuations.

The fluctuations may be associated with the presence of superexpansion in the following way (for details, see in 't Zand et al. 2011). When superexpansion is observed, an optically thick shell is thought to expand from the neutron star and skim the accretion disk within seconds. The shell can disturb the disk. The inner 10^2 km of the disk may be swept up due to the large ram pressure of the shell (we note that the expansion is fast, up to a few tens of percent of the speed of light), as might be the disk surface of inner 10^{3-4} km. The disk will resettle on a viscous timescale, but not before the Eddington-limited phase and the associated radiation pressure has ended. It is possible that the wind and radiation pressure of the regular photospheric expansion magnifies the disturbances imposed by the passing shell, and it will do so more if the expansion phase lasts longer.

The disturbance will be characterized by a vertical structure on the disk. This may be envisaged as clouds. Such highly ionized clouds may backscatter burst photons into the line of sight, when at the far side of the neutron star as seen by the observer, yielding upward fluctuations. Conversely, the cloud may scatter photons out of the line of sight when it is in the line of sight. Since the observed amplitudes of the fluctuations are so high, only one cloud can be active at a time. This model (some simple calculations were performed in in 't Zand et al. 2011) does not explain the occurrence of two types of variability. The fast fluctuations must originate closer to the neutron star than the slow dips, nor does it explain why these two types of variability happen after each other (slow after fast).

The observational data do not change this picture. The fact that the low-energy flux does not show such a high amplitude and that the best data from IGR J17062–6143 indicates a 1 keV emission feature as the culprit suggests that this may be due to a different emission region for the low-energy flux than for the high-energy flux. That would be consistent with the general idea that the accretion flow around neutron stars consists of multiple components, namely accretion disk, accretion disk corona, disk wind, and/or jet (for a recent review of similar accretion flows around black holes and further references, see, e.g., Blaes 2014), all with different regions and sizes.

7.2. Is the burst from SAX J1712.6–3739 on August 14, 2014, a superburst?

The e-folding decay time of the event from SAX J1712.6–3739 on August 14, 2014, of ~ 0.8 h is comparable to that of the shortest of 27 detected superbursts (in 't Zand et al. 2017; Iwakiri et al. 2018). The four shortest superbursts have e-folding decay times of 0.7 and 1.0 h for superbursts from GX 17+2, 0.5 h for one from 4U 1820–30 and 1.2 h for one from Ser X-1). The particular event from 4U 1820–30 is not thought

to be a superburst (Serino et al. 2016). GX 17+2 and Ser X-1 have, at the times of the superbursts, accretion rates in excess of 20% of Eddington. This is unlike SAX J1712.6–3739. Considering that some characteristics of the event from SAX J1712.6–3739 are consistent with the longest intermediate-duration bursts (superexpansion, a long PRE phase, low accretion rate; see, e.g., Table 4), we think it more likely that it is a long intermediate-duration bursts, in other words a flash of a thick helium pile instead of a thick carbon pile. This conclusion is identical to that drawn for other long bursts from SAX J1712.6–3739 (e.g., Kuulkers 2009; Iwakiri et al. 2018).

An increasing number of bursts have been identified, not only in this study, that have durations on the short end of the superburst distribution and on the long end of the distribution for intermediate-duration bursts. This gives rise to uncertainty in superburst identifications, not only for the burst from SAX J1712.6–3739, but also for IGR J1706–6143 (Iwakiri et al. 2015; Keek et al. 2017), 4U 1820–30, and SLX 1735–269 (Serino et al. 2016, 2017), among others. They can either be superbursts in high accretion rate systems or intermediate-duration bursts on cold neutron stars. It depends on the temperature of the neutron star and the characteristics of the bursts. The data sets on these diagnostics are, unfortunately, scarce and progress in their understanding requires better data sets that are hard to obtain because of their rarity.

8. Summary and conclusion

We found five bursts in the *Swift* data with eclipse-like features and/or strong fluctuations during their decay. The five bursts are discussed in detail and are from 4U 1850–087, Swift J1734.5–3027, IGR J17062–6143, and SAX J1712.6–3739. Seven additional bursts from the literature show similar features. We provide a table with information about all twelve bursts, their variabilities, and general properties of the source.

We find that the typical timescale of the fluctuations is 1–50 s and the amplitude $\sim 70\%$ above and below the burst decay trend. The variabilities (fluctuations and eclipse-like features) almost always occur after the PRE-phase.

The fluctuations show similar spectral characteristics such as an emission line around ~ 1 keV. The spectrum does not change, except in total emission, between upward and downward fluctuations. The emission from this line is stronger for the downward fluctuations.

As previously suggested by in 't Zand et al. (2011), the fluctuations are possibly due to a disturbed accretion disk, which is likely caused by a combination of an expanding shell and a near-Eddington flux. These causes provide an explanation for the variabilities seen in these 12 bursts. The validity of this suggestion needs to be verified through modeling the interaction of shells, winds and radiation pressure and the accretion disk, using as constraints the superexpansive character of the bursts and the long Eddington-limited flux. We suggest that such a theoretical study should investigate the similarity with the instabilities seen in flags driven by laminar wind flows.

Acknowledgements. We thank the *Swift* Team for their long-lasting support of a wonderful mission for burst science, not only gamma-ray bursts, but also X-ray bursts. We are grateful to Neil Gehrels and his team for their willingness to open up *Swift* automatic slewing to X-ray bursts, which resulted in the interesting findings presented here. May Neil Gehrels rest in peace. We thank Motoko Serino and Wataru Iwakiri for providing the MAXI light curve for SAX J1712.6–3739 at our request, and Tadayasu Dotani, Ken Ebisawa, and Moto Kokubun for providing the light curve of M15 X-2. ND is supported by a Vidi grant from the Netherlands Organization for Scientific Research (NWO).

References

- Arnaud, K. A. 1996, in *Astronomical Data Analysis Software and Systems V*, eds. G. H. Jacoby, & J. Barnes, *ASP Conf. Ser.*, **101**, 17
- Barrière, N. M., Krivonos, R., Tomsick, J. A., et al. 2015, *ApJ*, **799**, 123
- Barthelmy, S. D., Barbier, L. M., Cummings, J. R., et al. 2005, *Space Sci. Rev.*, **120**, 143
- Barthelmy, S. D., Burrows, D. N., D'Elia, V., et al. 2013, *GRB Coordinates Network, Circular Service, No. 14355*, 14355
- Barthelmy, S. D., Kennea, J. A., Marshall, F. E., Melandri, A., & Sbarufatti, B. 2017a, *GRB Coordinates Network, Circular Service, No. 20970*, 20970
- Barthelmy, S. D., Beardmore, A. P., Burrows, D. N., et al. 2017b, *GRB Coordinates Network, Circular Service, No. 21369*, 21369
- Bassa, C. G., Jonker, P. G., in 't Zand, J. J. M., & Verbunt, F. 2006, *A&A*, **446**, L17
- Blaes, O. 2014, *Space Sci. Rev.*, **183**, 21
- Bozzo, E., Ferrigno, C., Kuulkers, E., et al. 2009, *ATel*, **2198**
- Bozzo, E., Romano, P., Falanga, M., et al. 2015, *A&A*, **579**, A56
- Breeveld, A. A., Burrows, D. N., Cummings, J. R., et al. 2015, *GRB Coordinates Network, Circular Service, No. 17479*, 17479
- Burrows, D. N., Hill, J. E., Nousek, J. A., et al. 2005, *Space Sci. Rev.*, **120**, 165
- Churazov, E., Sunyaev, R., Revnivtsev, M., et al. 2007, *A&A*, **467**, 529
- Cocchi, M., Bazzano, A., Natalucci, L., et al. 2001, *A&A*, **378**, L37
- Cumming, A., & Bildsten, L. 2001, *ApJ*, **559**, L127
- Cumming, A., Macbeth, J., in 't Zand, J. J. M., & Page, D. 2006, *ApJ*, **646**, 429
- Cummings, J. R., Gehrels, N., Malesani, D., Marshall, F. E., & Sbarufatti, B. 2014, *GRB Coordinates Network, Circular Service, No. 16707*, 16707
- David, P., Goldwurm, A., Murakami, T., et al. 1997, *A&A*, **322**, 229
- De Falco, V., Kuiper, L., Bozzo, E., et al. 2017, *A&A*, **603**, A16
- Degenaar, N., & Wijnands, R. 2010, *A&A*, **524**, A69
- Degenaar, N., & Wijnands, R. 2013, in *Neutron Stars and Pulsars: Challenges and Opportunities after 80 Years*, ed. J. van Leeuwen, *IAU Symp.*, **291**, 141
- Degenaar, N., Jonker, P. G., Torres, M. A. P., et al. 2010, *MNRAS*, **404**, 1591
- Degenaar, N., Linares, M., Altamirano, D., & Wijnands, R. 2012a, *ApJ*, **759**, 8
- Degenaar, N., Altamirano, D., & Wijnands, R. 2012b, *ATel*, **4219**
- Degenaar, N., Miller, J. M., Wijnands, R., Altamirano, D., & Fabian, A. C. 2013, *ApJ*, **767**, L37
- Degenaar, N., Wijnands, R., Reynolds, M. T., et al. 2014, *ApJ*, **792**, 109
- Degenaar, N., Wijnands, R., Miller, J. M., et al. 2015, *J. High Energy Astrophys.*, **7**, 137
- Degenaar, N., Pinto, C., Miller, J. M., et al. 2017, *MNRAS*, **464**, 398
- Degenaar, N., Ballantyne, D. R., Belloni, T., et al. 2018, *Space Sci. Rev.*, **214**, 15
- Dieball, A., Knigge, C., Zurek, D. R., et al. 2005, *ApJ*, **634**, L105
- Falanga, M., Chenevez, J., Cumming, A., et al. 2008, *A&A*, **484**, 43
- Fiocchi, M., Bazzano, A., Ubertini, P., & De Cesare, G. 2008a, *A&A*, **477**, 239
- Fiocchi, M., Bazzano, A., Ubertini, P., et al. 2008b, *A&A*, **492**, 557
- Galloway, D. K., & Keek, L. 2017, in *ArXiv e-prints* [arXiv:1712.06227]
- Galloway, D. K., Muno, M. P., Hartman, J. M., Psaltis, D., & Chakrabarty, D. 2008, *ApJS*, **179**, 360
- Gehrels, N., Chincarini, G., Giommi, P., et al. 2004, *ApJ*, **611**, 1005
- Gotthelf, E. V., & Kulkarni, S. R. 1997, *ApJ*, **490**, L161
- Grindlay, J., Gursky, H., Schnopper, H., et al. 1976, *ApJ*, **205**, L127
- Hansen, C. J., & van Horn, H. M. 1975, *ApJ*, **195**, 735
- Harris, W. E. 1996, *AJ*, **112**, 1487
- Heinke, C. O., Bahramian, A., Degenaar, N., & Wijnands, R. 2015, *MNRAS*, **447**, 3034
- Hernandez Santisteban, J. V., Cuneo, V., Degenaar, N., et al. 2018, *MNRAS*, submitted [arXiv:1801.03006]
- Homer, L., Charles, P. A., Naylor, T., et al. 1996, *MNRAS*, **282**, L37
- Horne, K. 1985, *MNRAS*, **213**, 129
- in 't Zand, J. 2017, in *7 Years of MAXI: Monitoring X-ray Transients, held 5–7 December 2016 at RIKEN*, eds. M. Serino, M. Shidatsu, W. Iwakiri, & T. Mihara (Saitama, Japan: RIKEN), 121
- in 't Zand, J. J. M., & Weinberg, N. N. 2010, *A&A*, **520**, A81
- in 't Zand, J., Heise, J., Bazzano, A., Cocchi, M., & Smith, M. J. S. 1999, *IAU Circ.*, **7243**
- in 't Zand, J. J. M., Verbunt, F., Kuulkers, E., et al. 2002, *A&A*, **389**, L43
- in 't Zand, J. J. M., Cumming, A., van der Sluys, M. V., Verbunt, F., & Pols, O. R. 2005, *A&A*, **441**, 675
- in 't Zand, J. J. M., Jonker, P. G., & Markwardt, C. B. 2007, *A&A*, **465**, 953
- in 't Zand, J. J. M., Bassa, C. G., Jonker, P. G., et al. 2008, *A&A*, **485**, 183
- in 't Zand, J. J. M., Galloway, D. K., & Ballantyne, D. R. 2011, *A&A*, **525**, A111
- in 't Zand, J. J. M., Galloway, D. K., Marshall, H. L., et al. 2013, *A&A*, **553**, A83
- in 't Zand, J. J. M., Cumming, A., Triemstra, T. L., Matejisen, R. A. D. A., & Bagnoli, T. 2014a, *A&A*, **562**, A16
- in 't Zand, J., Linares, M., & Markwardt, C. 2014b, *ATel*, **5972**
- in 't Zand, J. J. M., Keek, L., & Cavecchi, Y. 2014c, *A&A*, **568**, A69
- in 't Zand, J. J. M., Visser, M. E. B., Galloway, D. K., et al. 2017, *A&A*, **606**, A130
- Iwakiri, W., Keek, L., Serino, M., et al. 2015, *ATel*, **8253**
- Iwakiri, W., Serino, M., Mihara, T., et al. 2018, *ATel*, **11422**
- Jager, R., Mels, W. A., Brinkman, A. C., et al. 1997, *A&AS*, **125**, 557
- Jenke, P. A., Linares, M., Connaughton, V., et al. 2016, *ApJ*, **826**, 228
- Joss, P. C. 1977, *Nature*, **270**, 310
- Juett, A. M., & Chakrabarty, D. 2003, *ApJ*, **599**, 498
- Juett, A. M., Psaltis, D., & Chakrabarty, D. 2001, *ApJ*, **560**, L59
- Keek, L., Iwakiri, W., Serino, M., et al. 2017, *ApJ*, **836**, 111
- Kennea, J. A., Altamirano, D., Evans, P. A., et al. 2012, *ATel*, **4192**
- Krimm, H. A., Holland, S. T., Corbet, R. H. D., et al. 2013, *ApJS*, **209**, 14
- Kuin, P., Page, K., Campana, S., & Zane, S. 2015, *ATel*, **7849**
- Kuulkers, E. 2009, *ATel*, **2141**
- Kuulkers, E., Homan, J., van der Klis, M., Lewin, W. H. G., & Méndez, M. 2002a, *A&A*, **382**, 947
- Kuulkers, E., in 't Zand, J. J. M., van Kerkwijk, M. H., et al. 2002b, *A&A*, **382**, 503
- Lewin, W. H. G., van Paradijs, J., & Taam, R. E. 1993, *Space Sci. Rev.*, **62**, 223
- Lin, J., & Yu, W. 2018, *ATel*, **11623**
- Linares, M., Watts, A. L., Wijnands, R., et al. 2009, *MNRAS*, **392**, L11
- Malesani, D., Kennea, J. A., Burrows, D. N., et al. 2013, *GRB Coordinates Network, Circular Service, No. 15172*, 15172
- Malesani, D., Palmer, D. M., & Ukwatta, T. N. 2015, *GRB Coordinates Network, Circular Service, No. 17686*, 17686
- Maraschi, L., & Cavaliere, A. 1977, in *X-ray Binaries and Compact Objects*, ed. K. A. van der Hucht, 127
- Markwardt, C. B., Cummings, J., & Krimm, H. 2008, *ATel*, **1616**
- Molkov, S., Revnivtsev, M., Lutovinov, A., & Sunyaev, R. 2005, *A&A*, **434**, 1069
- Muno, M. P., Baganoff, F. K., & Arabadjijs, J. S. 2003, *ApJ*, **598**, 474
- Negoro, H., Kohama, M., Serino, M., et al. 2016, *PASJ*, **68**, S1
- Nelson, L. A., Rappaport, S. A., & Joss, P. C. 1986, *ApJ*, **304**, 231
- Palmer, D. 2011, *ATel*, **3663**
- Papitto, A., Bozzo, E., Ferrigno, C., et al. 2013a, *ATel*, **4959**
- Papitto, A., Ferrigno, C., Bozzo, E., et al. 2013b, *Nature*, **501**, 517
- Parikh, A. S., Wijnands, R., Degenaar, N., et al. 2017, *MNRAS*, **468**, 3979
- Remillard, R. A., & Levine, A. M. 2008, *ATel*, **1853**
- Revnivtsev, M. G., Kniazev, A., Karasev, D. I., Berdnikov, L., & Barway, S. 2013, *Astron. Lett.*, **39**, 523
- Ricci, C., Beckmann, V., Carmona, A., & Weidenspointner, G. 2008, *ATel*, **1840**
- Romano, P., Campana, S., Chincarini, G., et al. 2006, *A&A*, **456**, 917
- Roming, P. W. A., Kennedy, T. E., Mason, K. O., et al. 2005, *Space Sci. Rev.*, **120**, 95
- Savonije, G. J., de Kool, M., & van den Heuvel, E. P. J. 1986, *A&A*, **155**, 51
- Serino, M., Shidatsu, M., Ueda, Y., et al. 2015, *PASJ*, **67**, 30
- Serino, M., Iwakiri, W., Tamagawa, T., et al. 2016, *PASJ*, **68**, 95
- Serino, M., Iwakiri, W., Tamagawa, T., et al. 2017, in *14th International Symposium on Nuclei in the Cosmos (NIC2016)*, eds. S. Kubono, T. Kajino, S. Nishimura, et al., **020304**
- Sidoli, L., La Palombara, N., Oosterbroek, T., & Parmar, A. N. 2005, *A&A*, **443**, 223
- Skinner, G. K., Willmore, A. P., Eyles, C. J., Bertram, D., & Church, M. J. 1987, *Nature*, **330**, 544
- Stella, L., Priedhorsky, W., & White, N. E. 1987, *ApJ*, **312**, L17
- Strohmayer, T., & Bildsten, L. 2006, *New Views of Thermonuclear Bursts (Compact Stellar X-ray Sources)*, **113**
- Strohmayer, T. E., & Baumgartner, W. H. 2010, *ATel*, **2717**
- Strohmayer, T. E., & Brown, E. F. 2002, *ApJ*, **566**, 1045
- Strohmayer, T., & Keek, L. 2017, *ApJ*, **836**, L23
- Strohmayer, T. E., Arzoumanian, Z., Bogdanov, S., et al. 2018, *ApJ*, **858**, L13
- Swank, J., & Markwardt, C. 2001, in *New Century of X-ray Astronomy*, eds. H. Inoue, & H. Kunieda, *ASP Conf. Ser.*, **251**, 94
- Swank, J. H., Becker, R. H., Boldt, E. A., et al. 1977, *ApJ*, **212**, L73
- Trap, G., Falanga, M., Goldwurm, A., et al. 2009, *A&A*, **504**, 501
- van den Eijnden, J., Degenaar, N., Pinto, C., et al. 2018, *MNRAS*, **475**, 2027
- van Paradijs, J., Dotani, T., Tanaka, Y., & Tsuru, T. 1990, *PASJ*, **42**, 633
- Wiersema, K., Russell, D. M., Degenaar, N., et al. 2009, *MNRAS*, **397**, L6
- Wijnands, R., Rol, E., Cackett, E., Starling, R. L. C., & Remillard, R. A. 2009, *MNRAS*, **393**, 126
- Wijnands, R., Parikh, A. S., Altamirano, D., Homan, J., & Degenaar, N. 2017, *MNRAS*, **472**, 559
- Worpel, H., Galloway, D. K., & Price, D. J. 2013, *ApJ*, **772**, 94
- Yan, Z., & Yu, W. 2015, *ApJ*, **805**, 87
- Yoon, D., Morsony, B., Heinz, S., et al. 2011, *ApJ*, **742**, 25
- Zhong, J., & Wang, Z. 2011, *ApJ*, **729**, 8

Appendix A: All *Swift* X-ray burst detections with event data

On March 31, 2018, we downloaded all XRT data concerning the 111 Galactic X-ray bursters known at the time, extracted light curves at 1 s resolution of all data, and searched for X-ray bursts. The data set consists of 15.2 Msec exposure. Particularly the four bursters that are in the field of view of the Galactic center (XMM J174457–2850.3, GRS 1741.9–2853, AX J1745.6–2901, and 1A 1742–289) were widely covered with about 2.1–2.2 Msec each. We found 90 X-ray bursts from 45 bursters. The numbers per burster are listed in Table A.1. *Swift* discovered 13 new bursters: the 6 *Swift* sources in the list plus IGR J00291+5934 (Kuin et al. 2015), MAXI J1647–227 (Kennea et al. 2012), XTE J1701–407 (Markwardt et al. 2008),

IGR J17062–6143 (Degenaar et al. 2012b), 1RXHJ173523.7–354013 (Degenaar et al. 2010), IGR J17511–3057 (Bozzo et al. 2009), and IGR J18245–2452 (Papitto et al. 2013a).

We provide a list of the 90 bursts detected with XRT in Table A.2, plus the 45 bursts that were detected with BAT and for which no XRT signal was found. This table includes the trigger numbers if appropriate, the trigger times if appropriate, the burst start times (estimated with an accuracy of a few seconds), and indications of the e-folding decay times in both BAT and XRT data, if appropriate. Furthermore, we list 41 BAT triggers on burster locations for which there is no clear signal in BAT. This includes image triggers that are less certain to involve X-ray bursts.

Figure A.1 shows the light curves for all 90 bursts that have XRT coverage.

Table A.1. Summary of all XRT observations of all 111 X-ray bursters until March 31, 2018.

Source	Exposure time (ksec)	No. bursts	Source	Exposure time (ksec)	No. bursts
IGR J00291+5934	50.8	1	IGR J17464–2811	63.9	0
4U 0513–40	38.8	0	IGR J17473–2721	7.0	1
4U 0614+09	463.5	2	SLX 1744–300	2.4	0
EXO 0748–676	311.2	2	SLX 1744–299	2.2	0
4U 0836–429	0	0	GX 3+1	5.2	0
2S 0918–549	25.3	0	IGR J17480–2446	210.8	0
4U 1246–588	13.7	1	EXO 1745–248	210.8	1
4U 1254–69	37.4	0	Swift J174805.3–244637	210.8	2
SAX J1324.5–6313	38.0	0	1A 1744–361	10.9	0
4U 1323–62	46.3	0	SAX J1748.9–2021	101.2	5
MAXI J1421–613	21.9	1	Swift J1749.4–2807	86.5	1
Cen X-4	142.6	0	IGR J17498–2921	87.3	2
Cir X-1	180.6	1	4U 1746–37	54.8	3
UW CrB	36.2	0	SAX J1750.8–2900	76.8	0
4U 1608–522	107.9	0	EXO 1747–214	0	0
MAXI J1621–501	23.7	0	GRS 1747–312	16.3	0
4U 1636–536	125.3	11	IGR J17511–3057	80.5	3
MAXI J1647–227	10.6	2	SAX J1752.3–3138	1.9	0
XTE J1701–462	177.2	0	SAX J1753.5–2349	20.5	0
XTE J1701–407	52.6	2	AX J1754.2–2754	52.1	1
MXB 1658–298	78.0	2	IGR J17597–2201	11.2	0
4U 1702–429	7.4	0	1RXS J180408.9–342058	115.3	6
IGR J17062–6143	137.9	1	SAX J1806.5–2215	105.9	1
4U 1708–23	10.4	0	2S 1803–245	0	0
4U 1705–32	19.8	0	SAX J1808.4–3658	353.7	1
4U 1705–44	8.7	0	XTE J1810–189	19.1	2
XTE J1709–267	32.4	0	SAX J1810.8–2609	13.8	1
XTE J1710–281	5.3	1	XTE J1812–182	2.2	0
4U 1708–40	0.5	0	XTE J1814–338	2.0	0
SAX J1712.6–3739	21.7	3	GX 13+1	25.7	0
2S 1711–339	2.8	0	4U 1812–12	13.2	0
RX J1718.4–4029	104.1	0	GX 17+2	121.7	0
1H 1715–321	1.1	0	Swift J181723.1–164300	21.9	0
IGR J17191–2821	9.9	1	SAX J1818.7+1424	33.1	0
XTE J1723–376	0.7	0	4U 1820–303	50.0	1
IGR J17254–3257	10.3	0	IGR J18245–2452	131.1	2
4U 1722–30	2.0	0	4U 1822–000	0	0
4U 1728–34	21.8	1	SAX J1828.5–1037	41.8	0
MXB 1730–335	111.3	3	GS 1826–24	51.7	2
KS 1731–260	0	0	XB 1832–330	5.1	0
Swift J1734.5–3027	60.3	1	Ser X-1	6.0	0
1RXH J173523.7–354013	39.7	1	Swift J185003.2–005627	27.0	1
SLX 1732–304	3.6	0	4U 1850–086	11.8	1
IGR J17380–3747	3.1	0	HETE J1900.1–2455	74.7	0
SLX 1735–269	14.7	1	XB 1905+000	0	0
4U 1735–444	114.1	5	Aql X-1	612.8	2
XTE J1739–285	16.6	1	XB 1916–053	54.7	0
SLX 1737–282	8.5	0	Swift J1922.7–1716	55.9	1
IGR J17445–2747	23.8	0	XB 1940–04	0	0
KS 1741–293	102.7	0	XTE J2123–058	0	0
XMM J174457–2850.3	2149.2	1	4U 2129+12	57.9	0
GRS 1741.9–2853	2149.2	2	XB 2129+47	0	0
AX J1745.6–2901	2190.7	2	Cyg X-2	144.0	1
1A 1742–289	2191.2	0	SAX J2224.9+5421	26.5	0
1A 1742–294	8.6	0	4U 1543–624	7.4	0
SAX J1747.0–2853	65.3	0			

Notes. These observations yielded 90 detections of X-ray bursts.

Table A.2. List of 134 X-ray bursts detections with *Swift* until March 31, 2018, for which event data is available.

Source	Date and time (UTC)	Det. ^a	Trigger id.	Time (MET) ^b (s)	MJD(UTC) ^b	BAT double peaked?	BAT dur. ^c (s)	XRT decay ^d (s)
4U 1702–429	2005-01-29 17:04:14	b	104039	128711053.70	53399.711277	Y	14	
4U 1812–12	2005-01-30 17:26:09	b	104090	128798768.38	53400.726493	Y	13	
EXO 0748–676	2005-02-12 16:56:54	x		129920221.71	53413.706192			26
EXO 0748–676	2005-02-12 20:00:28	x		129931234.71	53413.833658			17
4U 1636–536	2005-02-13 22:11:40	b	106034	130025499.90	53414.924774		14	
4U 1728–34	2005-02-14 09:08:32	b	106070	130064911.49	53415.380927		4	
4U 1702–429	2005-02-17 14:57:15	b	106276	130345033.98	53418.623086	Y	11	
4U 1636–536	2005-02-22 13:48:58	b	106666	130772936.96	53423.575666		6	
4U 1702–429	2005-02-23 08:30:40	b	106724	130840239.36	53424.354629		14	
4U 1812–12	2005-02-24 12:40:46	sl	106799	130941645.31	53425.528309	Y	21	
4U 1812–12	2005-03-14 03:18:38	b	110772	132463117.31	53443.137938	Y	16	
4U 1636–536	2005-07-02 09:01:17	b	143840	141987676.42	53553.375889		8	
4U 1702–429	2005-07-03 20:29:23	b	144067	142115362.24	53554.853734		11	
4U 1728–34	2005-07-21 11:14:30	b	147029	143637270.40	53572.468412	Y	10	
SLX 1735–269	2005-07-28 21:36:40	b	147919	144279400.00	53579.900467		11	
HETE J1900.1–2455	2005-08-17 12:19:58	b	150823	145973997.70	53599.513866	Y	19	
HETE J1900.1–2455	2005-08-28 15:09:37	b	152451	146934576.32	53610.631674	Y	17	
XTE J1739–285	2005-10-31 20:39:19	x		152483980.62	53674.860648			3
XTE J1723–376	2006-02-12 23:42:39	b	181323	161480560	53778.987951		5	
SAX J1747.0–2853	2006-03-25 00:53:03	b	202662	164940784	53819.036839			
2S 0918–549	2006-04-15 03:38:09	b	205373	166765090.62	53840.151499		12	
Swift J1749.4–2807	2006-06-02 23:54:34	sl	213190	170985275.14	53888.996226		20	7
GRS 1741.9–2853	2006-06-04 09:40:27	x		171106844.23	53890.403100			11
4U 1636–536	2006-06-11 15:09:47	bx		171731387.10	53897.6231802		8	11
4U 1636–536	2006-06-12 05:24:08	bx		171782648.10	53898.225101		10	9
4U 1246–588	2006-08-11 02:59:55	sl	223918	176957996.86	53958.124948		70	
Aql X-1	2006-08-15 11:07:18	bx		177332850.70	53962.463408	Y	10	16
SAX J1747.0–2853	2006-08-19 14:43:20	b	225393	177691401.86	53966.613431		11	
4U 0614+09	2006-10-21 09:02:00	b	234849	183114121.98	54029.376394		40	
GRS 1741.9–2853	2007-01-22 06:12:58	b	257213	191139180.16	54122.259010		13	
AX J1745.6–2901	2007-02-16 22:59:18	bx		193359575.23	54147.957857		10	11
GRS 1741.9–2853	2007-03-05 20:19:00	bx		194818757.23	54164.846537	Y	10	15
4U 0614+09	2007-03-30 08:53:21	b	273106	196937603.14	54189.370385		23	
SLX 1744–299	2007-04-26 06:03:50	b	277191	199260232	54216.252663		20	
IGR J17191–2821	2007-05-01 13:20:53	x		199718455.33	54221.556173			17
4U 1702–429	2007-05-16 21:00:25	b	279418	201042026.75	54236.875287		10	
XB 1832–330	2007-05-30 07:44:15	b	280846	202203857.47	54250.322401		7	
AX J1754.2–2754	2007-07-12 09:12:28	x		205924368.81	54293.383660			–
SAX J1810.8–2609	2007-08-05 11:27:26	sl	287042	208006048.51	54317.477389	Y	23	84
SAX J1810.8–2609	2007-09-01 11:19:26	b	288384	210338367.94	54344.471826	Y	22	
SAX J1810.8–2609	2007-09-16 15:54:17	b	291218	211650858.75	54359.662691	Y	12	
Aql X-1	2007-09-19 07:56:35	b	291524	211881397.50	54362.330964	Y	5	
SAX J1810.8–2609	2007-09-27 15:09:44	b	292421	212598586.50	54370.631762		5	
XTE J1810–189	2008-03-18 22:32:53	sl	306737	227572375.17	54543.939497		10	–
XTE J1810–189	2008-03-21 14:56:33	bx		227804200.86	54546.622613		20	31
IGR J17473–2721	2008-03-31 09:03:33	sl	308196	228647016.13	54556.377470	Y	25	17
SAX J1750.8–2900	2008-04-27 18:35:45	b	310319	231014147.33	54583.774822		8	
1RXH J173523.7–354013	2008-05-14 10:32:37	sl	311603	232453960.	54600.439320		240	289
4U 1636–536	2008-05-19 22:21:23	x		232928483.10	54605.931524			14
XTE J1701–407	2008-07-17 13:30:00	sl	317205	237994202.69	54664.562497		125	119
XTE J1701–407	2008-07-27 22:31:20	sl	318166	238890682.82	54674.938424		15	<40
SAX J1808.4–3658	2008-09-24 20:14:24	b	325827	243980067.33	54733.843336	Y	15	
MXB 1730–335	2009-03-05 13:28:15	x		257952505.27	54895.561292			11
4U 1820–303	2009-06-06 09:28:19	b	354224	265973303.55	54988.394661	Y	6	
4U 1820–303	2009-06-06 12:43:33	bx		265985018.58	54988.530252		4	7

Notes. At the bottom, an additional 41 BAT triggers (without slew) on burst source locations are listed that reveal no clear burst signal in BAT. ^(a)“b” = BAT detection, “x” = XRT detection, “sl” = BAT trigger and AT, “n” = BAT nor XRT detection. ^(b)The times refer to the trigger time for those that triggered BAT (i.e., with a trigger ID) or to the burst onset time for the others. The trigger times were extracted from gcn.gsfc.nasa.gov/swift_grbs.html. ^(c)The duration of the BAT signal, judged by eye, only if detected. ^(d)The exponential decay time of the XRT signal, fitted, only if detected.

Table A.2. continued.

Source	Date and time (UTC)	Det. ^a	Trigger id.	Time (MET) ^b (s)	MJD(UTC) ^b	BAT double peaked?	BAT dur. ^c (s)	XRT decay ^d (s)
IGR J17511–3057	2009-09-14 00:50:31	bx		274582236.37	55088.035084		10	10
IGR J17511–3057	2009-09-15 17:17:13	bx		274727838.37	55089.720292		20	18
IGR J17511–3057	2009-09-30 18:31:57	sl	371210	276028321.66	55104.772182		20	15
GS 1826–24	2009-10-21 17:44:55	x		277839902.24	55125.739529			82
4U 1728–34	2009-10-30 10:19:42	bx		278590782.29	55134.430355		35	33
Aql X-1	2009-11-16 02:03:24	bx		280029816.70	55151.085699		15	22
4U 1850–086	2010-02-16 06:07:42	b	412503	287993267.26	55243.255344		6	
SAX J1712.6–3739	2010-07-01 14:55:41	sl	426405	299688946.69	55378.621999		30	119
IGR J17464–2811	2010-08-13 21:03:30	b	431582	303426216	55421.877430		110	
1E 1145.1–6141	2011-04-03 02:38:09	b	450610	323491096	55654.109829		5	
XTE J1810–189	2011-06-19 00:59:37	sl	455640	330137984.	55731.041400		400	53
Swift J185003.2–005627	2011-06-25 00:06:08	sl	456014	330653174.72	55737.004255		40	80
IGR J17498–2921	2011-08-18 11:22:34	x		335359374.87	55791.474009			8
IGR J17498–2921	2011-08-28 10:12:04	x		336219144.87	55801.425051			14
KS 1741–293	2011-09-01 12:07:22	b	502024	336571649.66	55805.505120		10	
SAX J1712.6–3739	2011-09-26 20:11:29	sl	504101	338760696.	55830.841303		315	200
Swift J1922.7–1716	2011-11-03 14:12:13	sl	506913	342022340.67	55868.591819	Y	50	106
Swift J1922.7–1716	2011-12-02 09:44:42	b	508855	344511889.47	55897.406040	Y	18	
MAXI J1647–227	2012-06-19 09:49:38	x		361792199.29	56097.409479			10
IGR J17062–6143	2012-06-25 22:42:32	sl	525148	362356960.	56103.946200		420	1186
MAXI J1647–227	2012-06-27 08:10:17	x		362477438.29	56105.340485			12
Swift J174805.3–244637	2012-07-17 21:05:29	bx		364251943.28	56125.878818		10	20
XMM J174457–2850.3	2012-08-11 04:43:54	sl	530588	366353043.33	56150.197151	Y	75	–
Swift J174805.3–244637	2012-08-13:09:13:34	sl	530808	366542023.81	56152.384424	Y	35	~100
Cyg X-2	2013-02-23 14:14:37	x		383321688.64	56346.593491			7
IGR J18245–2452	2013-03-30 15:10:38	sl	552369	386349048.	56381.632380		130	–
IGR J18245–2452	2013-04-07 22:15:21	bx		387065731.77	56389.927331		20	43
Swift J1734.5–3027	2013-09-01 09:13:17	sl	569022	399719608.	56536.384225		155	188
MAXI J1421–613	2014-01-18 08:39:20	sl	584155	411727171.2	56675.360664	Y	15	9
4U 1746–37	2014-02-16 19:18:41	x		414271134.68	56704.804644			12
4U 1746–37	2014-02-22 19:07:59	x		414788892.68	56710.797213			9
4U 1746–37	2014-02-22 20:40:29	x		414794442.68	56710.861450			13
4U 1735–444	2014-02-23 01:46:51	bx		414812824.26	56711.074210		5	12
4U 1735–444	2014-02-23 14:36:45	x		414859018.26	56711.608863			9
4U 1735–444	2014-02-23 16:16:39	bx		414865012.26	56711.678238		5	7
4U 1735–444	2014-02-24 08:10:48	x		414922261.26	56712.340842			10
4U 1735–444	2014-02-24 14:19:45	x		414944398.26	56712.597058			8
4U 1850–086	2014-03-10 21:05:00	sl	591237	416178312.	56726.878475		840	1999
GS 1826–24	2014-06-24 23:46:16	x		425346383.24	56832.990467			10
SAX J1712.6–3739	2014-08-18 17:10:04	sl	609878	430074616.	56887.715319		>800	42
4U 0614+09	2014-12-31 08:52:27	bx		441708760.80	57022.369764		15	26
1RXS J180408.9–342058	2015-02-06 21:24:14	x		444950668.12	57059.891840			58
4U 0614+09	2015-02-19 16:42:24	sl	631747	446056956.93	57072.696108		6	11
1RXS J180408.9–342058	2015-02-21 20:36:20	x		446243794.12	57074.858576			33
1RXS J180408.9–342058	2015-02-22 01:10:45	bx		446260258.12	57075.049132			36
1RXS J180408.9–342058	2015-02-26 02:48:18	x		446611711.12	57079.116875			37
SAX J1748.9–2021	2015-02-26 21:47:19	x		446680052.25	57079.907859			14
1RXS J180408.9–342058	2015-03-06 02:12:47	x		447300781.12	57087.092222			48
SAX J1748.9–2021	2015-03-09 01:57:46	bx		447559079.25	57090.081783			16
SAX J1748.9–2021	2015-03-16 05:26:37	x		448176410.25	57097.226818			27
EXO 1745–248	2015-03-25 05:06:02	x		448952776.28	57106.212533			10
1RXS J180408.9–342058	2015-03-31 23:44:56	bx		449538310.12	57112.989548			59
SAX J1748.9–2021	2015-04-06 10:26:22	bx		450008795.25	57118.434977			30
SAX J1808.4–3658	2015-04-11 19:36:25	sl	637765	450473798.66	57123.816959		25	46
SLX 1735–269	2015-04-18 00:20:55	x		451009273.70	57130.014526			3
MXB 1730–335	2015-05-30 01:45:51	x		454643161.27	57172.073515			21
SAX J1748.9–2021	2015-06-23 22:42:09	b	645944	456792142.4	57196.945933		10	
IGR J00291+5934	2015-07-25 02:12:05	sl	650221	459483139.84	57228.091724	Y	20	128
4U 1636–536	2015-09-05 18:35:23	x		463170923.10	57270.774580			16
MXB 1658–298	2015-09-09 10:07:54	x		463486090.72	57274.422159			14
SAX J1750.8–2900	2015-10-16 01:25:59	b	659734	466651574.53	57311.059714		12	

Table A.2. continued.

Source	Date and time (UTC)	Det. ^a	Trigger id.	Time (MET) ^b (s)	MJD(UTC) ^b	BAT double peaked?	BAT dur. ^c (s)	XRT decay ^d (s)
AX J1745.6–2901	2016-02-10 21:07:15	x		476831252.23	57428.880044			–
MXB 1658–298	2016-04-18 19:09:33	x		482699389.72	57496.798305			41
XTE J2123–058	2016-05-19 06:15:59	b	686845	485331376	57527.261108		10	
Cir X-1	2016-09-18 14:05:27	x		495900327.20	57649.587128			4
XTE J1710–281	2017-02-24 17:01:09	x		509648488.62	57808.709143			14
SAX J1806.5–2215	2017-04-01 19:00:53	sl	745022	512766072.	57844.792281		250	107
Swift J181723.1–164300	2017-07-28 16:57:58	sl	765081	522953897.41	57962.706921	Y	15	
Swift J181723.1–164300	2017-07-30 21:32:05	b	765422	523143144.45	57964.897280		8	
4U 1636–536	2017-08-03 05:25:59	x		523430759.10	57968.226385			21
MXB 1730–335	2017-08-26 21:15:15	x		525474925.27	57991.885598			8
4U 1636–536	2017-09-08 08:53:02	x		526553582.10	58004.370170			21
4U 1636–536	2017-09-14 17:44:23	bx		527103863.10	58010.739163		20	27
4U 1636–536	2017-09-17 04:52:32	x		527316752.10	58013.203156			16
4U 1636–536	2017-09-23 08:56:56	bx		527849816.10	58019.372878		20	13
4U 1636–536	2017-09-26 15:08:56	x		528131336.10	58022.631212			9
SAX J1748.9–2021	2017-10-05 19:32:22	bx		528924755.25	58031.814144			20
4U 1636–536	2017-10-23 09:26:11	bx		530443571.10	58049.393191		15	11
XTE J701–407	2018-03-09 18:20:35	b	813449	542312456.	58186.764299		150	
4U 0836–429	2005-01-06 16:59:00	n	101731					
Cyg X-2	2005-02-05 07:08:18	n	104695					
XB 1916–053	2005-02-26 01:29:30	n	106912					
4U 1735–44	2005-03-17 17:57:54	n	111378					
4U 1636–536	2005-03-20 19:28:56	n	111765					
IGR J17473–2721	2005-06-23 20:56:56	n	142554					
GS 1826–24	2005-06-24 21:03:28	n	142667					
GX 13+1	2005-07-09 09:35:20	n	145011					
4U 1746–37	2005-07-26 19:33:36	n	147857					
1E 1145.1–6141	2005-08-13 04:40:48	n	150131					
EXO 0748–676	2005-10-06 13:52:40	n	158539					
SLX 1737–282	2006-02-01 06:06:39	n	179811					
XTE J1701–462	2006-03-15 18:50:22	n	201721					
SAX J1747.0–2853	2006-03-28 13:50:14	n	203045					
XB 1832–330	2006-04-08 13:15:42	n	204415					
XTE J1701–462	2006-06-02 06:23:10	n	213056					
XTE J1701–462	2006-06-25 10:07:26	n	215987					
MXB 1730–335	2006-07-01 18:45:33	n	216664					
SAX J1808.4–3658	2008-09-24 00:37:16	n	325730					
IGR J17480–2446	2010-10-13 19:27:21	n	436241					
IGR J17480–2446	2010-10-28 22:35:21	n	437313					
IGR J17480–2446	2010-10-31 09:52:01	n	437466					
4U 1608–522	2011-08-12 03:24:40	n	500082					
GX 17+2	2011-08-12 05:40:32	n	500093					
GS 1826–24	2011-08-12 07:08:16	n	500108					
SAX J1808.4–3658	2011-11-04 02:55:12	n	506961					
1E 1145.1–6141	2012-04-10 17:59:52	n	519850					
IGR J17480–2446	2012-07-13 14:16:54	n	526511					
IGR J17480–2446	2012-07-16 20:59:50	n	526892					
SAX J1828.5–1037	2012-10-10 23:57:42	n	535733					
GX 17+2	2013-02-26 22:17:01	n	549824					
SAX J1806.5–2215	2013-06-20 02:21:57	n	558631					
Cyg X-2	2013-09-08 16:39:48	n	570069					
2S 1803–245	2014-11-14 07:32:03	n	618556					
1RXS J180408.9–342058	2015-01-31 21:14:18	n	629206					
1RXS J180408.9–342058	2015-02-06 20:45:14	n	630047					
SAX J1748.9–2021	2015-02-20 23:38:50	n	631946					
IGR J17480–2446	2015-04-05 18:15:06	n	637212					
IGR J00291+5934	2015-07-24 05:23:37	n	650140					
Ser X-1	2016-03-05 20:42:32	n	677890					
Swift J1922.7–1716	2017-08-01 17:03:16	n	765783					

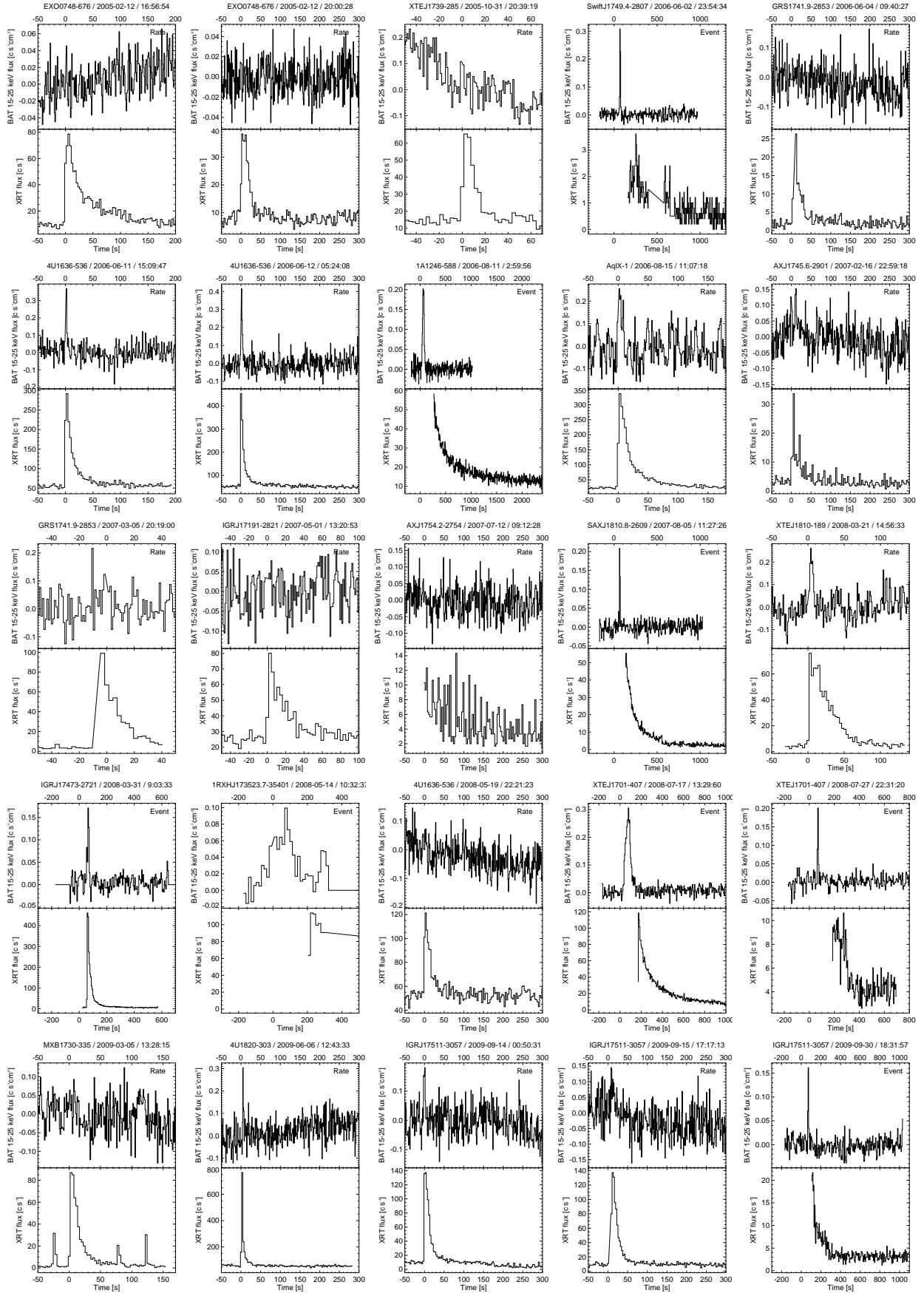


Fig. A.1. BAT (upper panels) and XRT light curves (lower panels) of all 90 X-ray bursts that have XRT coverage. The BAT light curves are labeled “Event” if they are from mask-tagged event data or “Rate” if they are inferred from rate meter data. In the latter case, the rate meter data have been pre-burst subtracted and divided by the photon-collecting area illuminated by the source that was identified on board.

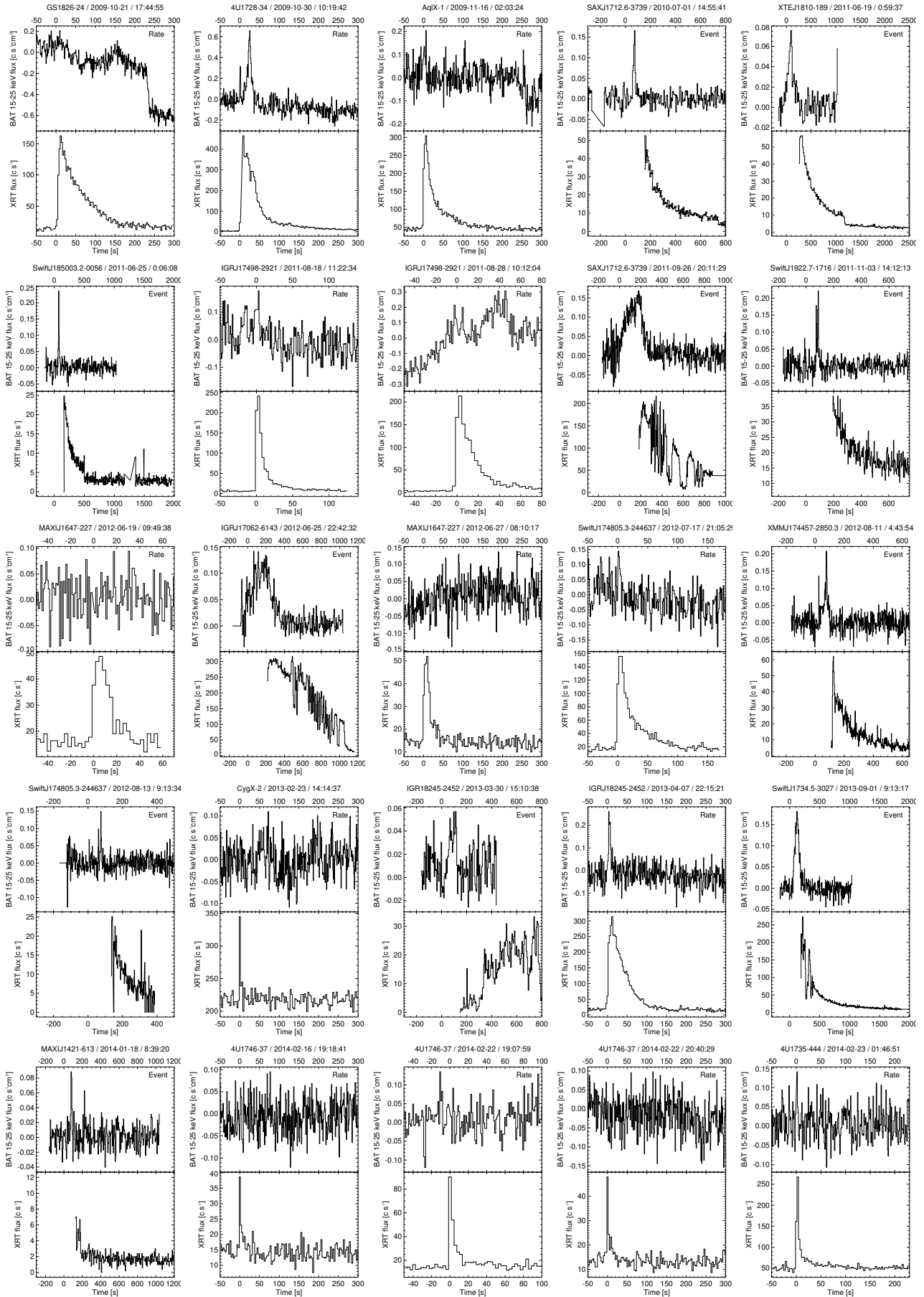


Fig. A.1. continued.

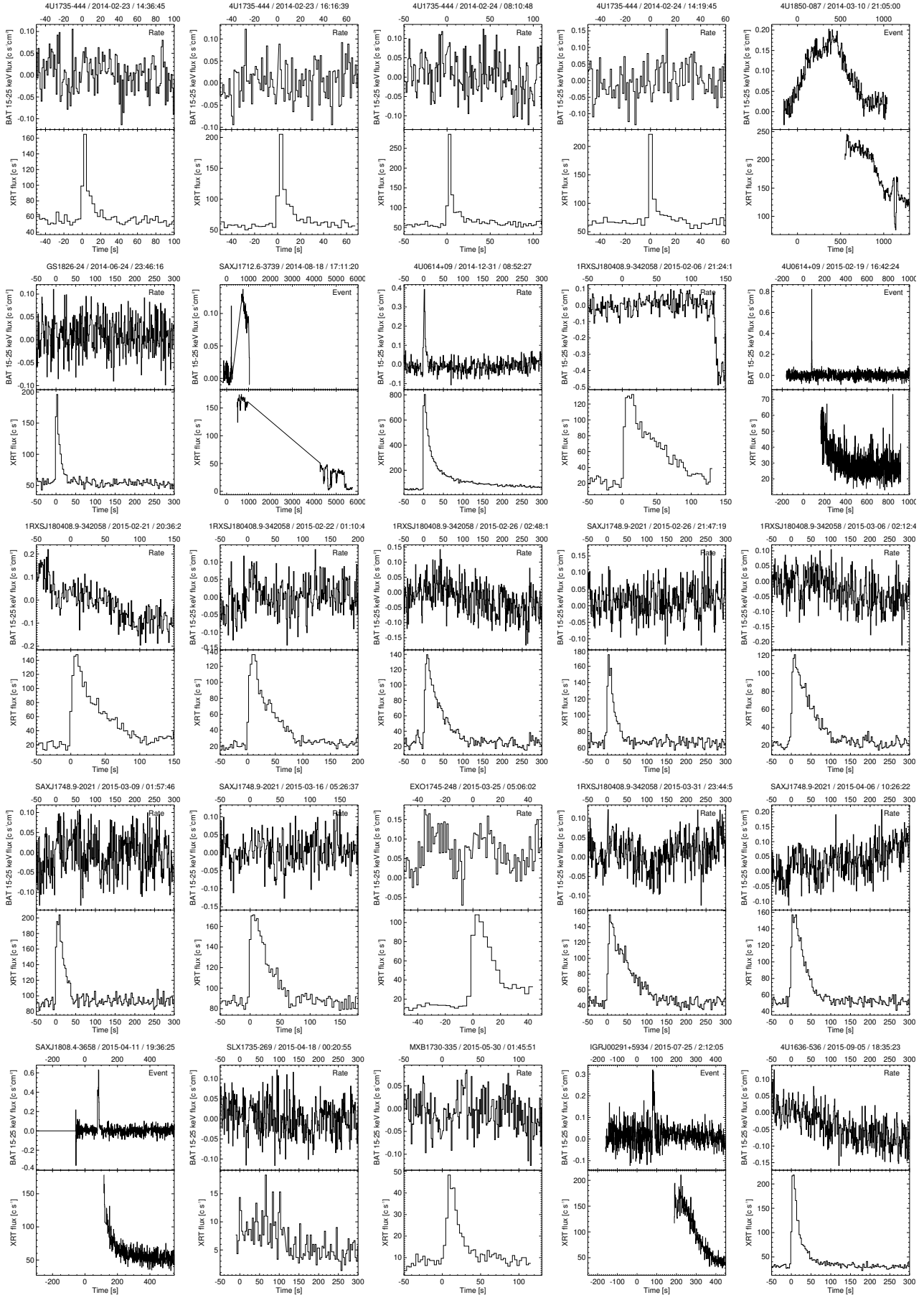


Fig. A.1. continued.

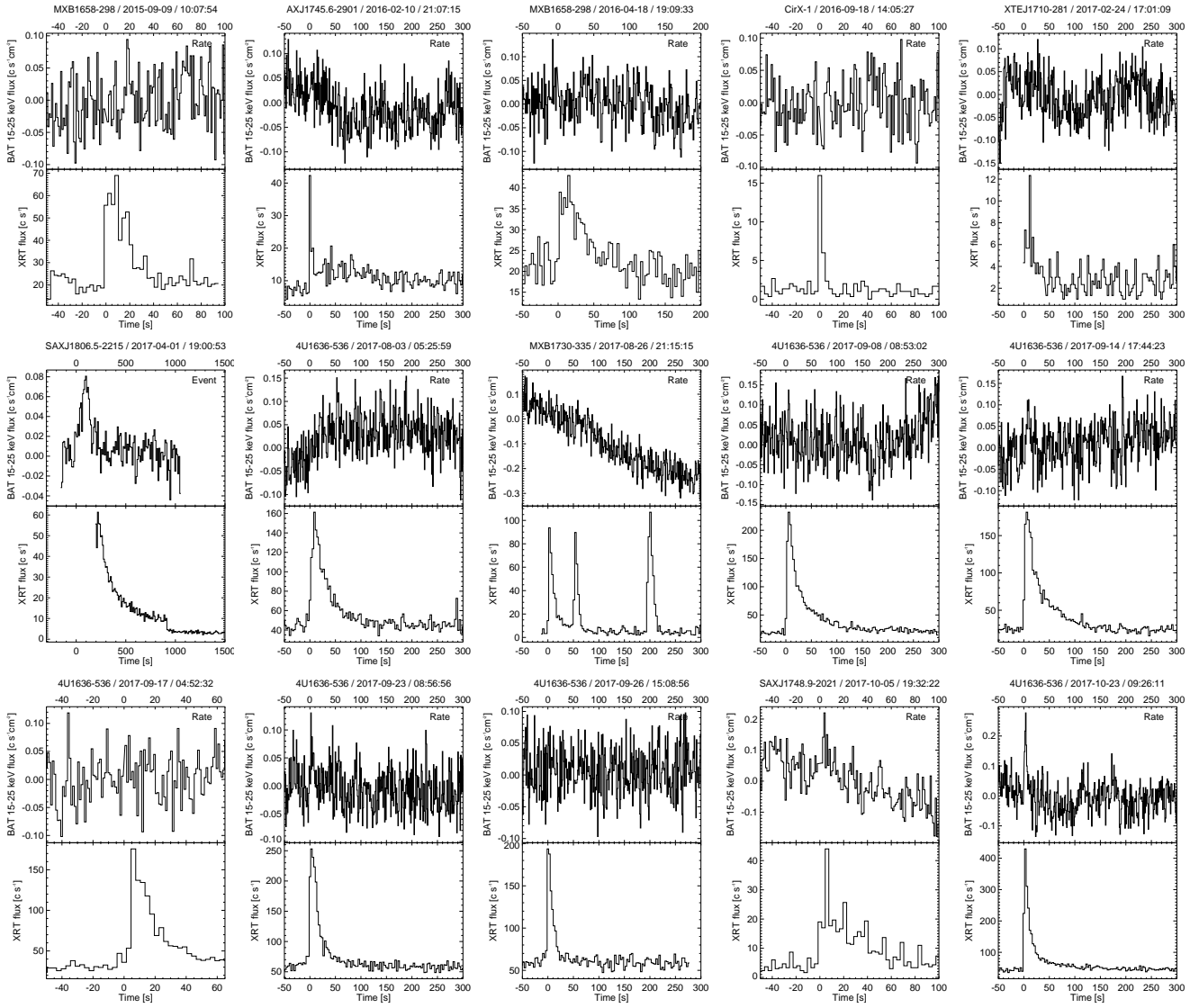


Fig. A.1. continued.